Incorporation of photo- and thermo-responsive *N*-salicylidene aniline derivatives into Cobalt and Zinc Layered Hydroxides

Varun Kumar,[a,*] *Quentin Evrard,*[a, †] *Cédric Leuvrey,*[a] *Marc Lenertz,*[a] *Yann Garcia,*[b] *Pierre Rabu,*[a] *Guillaume Rogez*[a,*]

a. Institut de Physique et Chimie de Strasbourg, CNRS – Université de Strasbourg, UMR7504, 23 rue du Loess, 67034 Strasbourg cedex 2, France

b. Institute of Condensed Matter and Nanosciences, Molecular Chemistry, Materials and Catalysis (IMCN/MOST), Université Catholique de Louvain, 1348 Louvain-la-Neuve, Belgium

varun.kumar@ipcms.unistra.fr

rogez@unistra.fr

ABSTRACT

In search for new multifunctional hybrid materials, and in order to investigate the influence of chemical modification on the possible synergy between properties, the carboxylate and sulfonate derivatives of photo and thermochromic N-salicylidene aniline were successfully inserted into Co(II) and Zn(II) based Layered Simple Hydroxides, resulting in four novel hybrids : Co-*N*-Sali-COO, Co-*N*-Sali-SO_3, Zn-*N*-Sali-COO and Zn-*N*-Sali-SO_3.

All synthesized hybrids adopt a double organic layered configuration which prevents the *cis-trans* photoisomerization ability of *N*-Sali-R molecules in the hybrids. However, the Zn hybrids exhibit fluorescence upon exposure to UV light due to the Excited State Intramolecular Proton Transfer (ESIPT) mechanism. The thermally stimulated keto-enol tautomerization of *N*-salicylidene aniline in the hybrids was related withed the changes in interlamellar spacings observed by temperature-dependent PXRD. This tautomerization process was prominently evident in the Co-N-Sali-SO_3 hybrid (about 11% increase in *d*-spacing upon decreasing the temperature to -180°C). Finally, the Co-N-Sali-R hybrids exhibit the typical magnetic behavior associated with Co(II)-based LSHs (ferrimagnetic ordering at T_N = 6.8 K and 7.7 K for Co-*N*-Sali-COO and Co-*N*-Sali-SO_3 respectively).

This work offers insights on isomerization in LSHs, and the ESIPT mechanism's potential in new luminescent materials and prospects for designing new multifunctional materials.

INTRODUCTION

Multifunctional materials hold immense promises for applications as they offer unique combination of physical, chemical or mechanical properties. The design and conception of such materials can be obtained using several routes. For instance, the controlled assembly of functional

nanosheets, also called nanoarchitectonics, constitutes a very rich field of research, with applications in (opto)electronics, sensors, energy storage or (photo)catalysis to quote just a few.[1,2] Another successful approach consists in associating two components, organic and inorganic within a single material.[3,4] The resulting organic-inorganic hybrid material may inherit the individual properties of its constituents, as well as possess a new property due to a synergistic interaction between the properties.[5,6] Organic-inorganic compounds are not just a physical mixture, but they are composites at the molecular scale where the constituents interact through weak or strong bonding (H-bonds, electrostatic interactions, iono-covalent bonding). Layered compounds represent prototypical models for such hybridization.[7–10] Indeed such materials are ideal candidates to facilitate hybridization by hosting a variety of organic compounds in their interlayer space *via* versatile chemical routes. Among layered materials, Layered Double Hydroxides (LDHs) with functional organic compounds have been extensively explored for catalysis,[11,12] flame-retardant,[13] photovoltaics,[14,15] CO_2 capture,[16] drug-delivery,[17,18] electrode materials,[19,20] combining photo-chromism and magnetism[9,21] *etc*.[22] However, despite being relatively easy to synthesize, hybrid LDHs present weak bonds between the organic intercalants and the inorganic host,[7] which somehow limits the possibility of synergy between the properties of the two subnetworks *via* through-space interactions. Other types of well-studied hybrid layered compounds such as metal oxalates[23–25] or hexathiohypodiphosphate[26,27] are also characterized by weak bonds between organic and inorganic moieties. With this respect, transition metal layered simple hydroxides can offer an alternative in the sense that inserted molecules are indeed grafted onto the inorganic layers by means of iono-covalent bonds.[7] Layered Simple Hydroxides (LSHs) are compounds of general formula $M^{2+}_x(OH^-)_{2x-ny}(A^{n-})_y \cdot zH_2O$ (with M = Mn^{2+}, Cu^{2+}, Ni^{2+} or $Zn^{2+}$and A^{n-} an anion that can be any molecule possessing an anchoring function (carboxylate, sulfate, sulfonate or phosphonate)

or a nitrate or halide. LSHs present essentially two types of structure of the inorganic layers. One type corresponds to LSHs exhibiting a simple brucite-like layer of metal ions in edge sharing octahedral sites, with the interlayer anion directly grafted to three octahedral shared vertices.[28–31] The other type differs from the first one by the fact that the octahedral layers present vacancies, with tetrahedral sites above and below these vacancies, resulting in triple-deck layers. These vacancies can be randomly distributed like in the case of cobalt hydroxy-chloride,[32–35] or have a specific ordering like in zinc hydroxy-nitrate.[36]

One key interest about LSHs is their structure flexibility and compositional multiplicity which make them versatile hosts for a variety of functional organic anions. One of the first examples results from the topotactic reaction of the zinc hydroxy-nitrate with aqueous metal chloride leading to the anion exchange from nitrate to chloride as well as a partial exchange of the zinc with the cobalt of nickel cations. Yet, the most studied LSH are the Cu and Co ones, which have been successfully functionalized by *n*-alkyl-(di)carboxylates,[37–41] *n*-alkyl-(di)sulfates and sulfonates,[42] stilbazolium carboxylates and sulfonate,[43] α,α'-oligothiophenecarboxylates,[44,45] oligophenylene-vinylenecarboxylates,[46] alkylphosphonates,[47] metal phthalocyanine tetrasulfonates[48] and salen-type complexes with carboxylate or sulfonate anchoring groups.[49–51]

Following the results obtained on the functionalization of magnetic LDHs by thermo[52] or photoresponsive[21] molecules, we have chosen to explore the grafting of photo and thermochromic molecules onto magnetic Co LSH *via* carboxylic or sulfonic acid anchoring groups, in order to investigate the influence of chemical grafting on the possible synergy between properties, which is indeed null[52] or limited[21] in the previous examples in hybrid LDHs.

For the purpose, we have chosen *N*-salicylidene aniline based molecules which present the ability to be thermo- and photo-switchable under three distinct forms (enol, *cis*-keto and

trans-keto form) within a three-color set in the solid-state as shown in Scheme 1.[53,54] Due to their photo-and thermo-chromic properties *N*-salicylidene aniline molecules have been hailed as candidates for several applications including non-linear optics,[55] catalysis,[56] pharmaceutical,[57] chemical sensing,[58] stimuli responsive polymers,[59] and optical data storage[60] among others. The enol form is usually colorless whereas *cis*-keto and *trans*-keto form can display colors from yellow to orange. The enol form of *N*-salicylidene aniline based molecules also emits fluorescence when irradiated with UV-light.

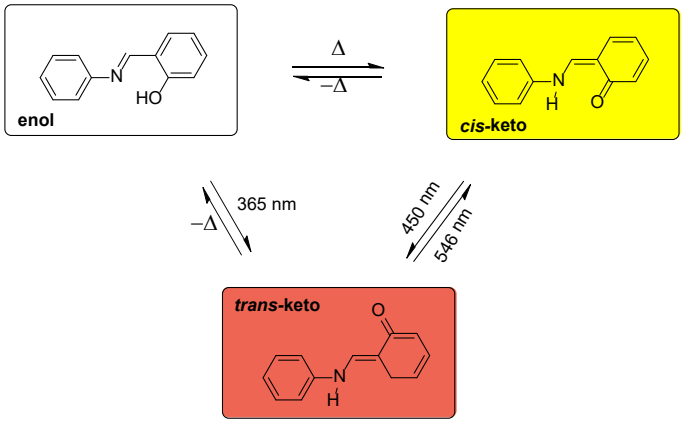

Scheme 1. Thermo and photo-isomerization of *N*-salicylidene aniline.

In order to better investigate the optical properties of the inserted *N*-salicylidene aniline molecules, we also inserted them in Zn-LSH, which is does not absorb light in the visible part of the spectrum. Herein, we describe the synthesis and characterization of four novel hybrid LSHs incorporating carboxylate and sulfonate derivatives of *N*-salicylidene aniline, *viz*. *N*-Sali-COO^- and *N*-Sali-SO_3^- (Scheme 2), $M_5(OH)_{10-x}$(*N*-Sali-R)$_x \cdot yH_2O$ where M = Co(II) and Zn(II) and R = -COO and -SO_3. In the following, the hybrid compounds will be referred to as Co-*N*-Sali-COO, Co-*N*-Sali-SO_3, Zn-*N*-Sali-COO, and Zn-*N*-Sali-SO_3.

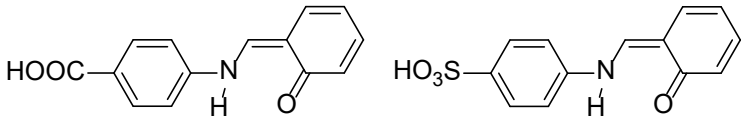

***N*-Sali-COOH** ***N*-Sali-SO_3H**

Scheme 2. Carboxylic and sulfonic acid derivatives of *N*-salicylidene aniline.

EXPERIMENTAL SECTION

Powder X-ray diffraction (PXRD) patterns were collected on a Bragg-Brentano geometry with a Bruker D8DISCOVER diffractometer (CuKα1 = 0.1540598 nm) equipped with a LynxEye detector discriminating in energy. Fourier Transform-Infra red spectra (FT-IR) were collected in ATR mode on a Perkin-Elmer SpectrumII spectrometer. Diffuse reflectance spectroscopy was performed with a Perkin-Elmer Lambda 950 spectrometer (spectra recorded in the reflection mode, using a 150 mm integrating sphere, with a resolution of 2 nm and a mean sampling rate of 200 $nm \cdot min^{-1}$). The emission spectra were recorded on a Fluorolog spectrometer (Horiba Jobin-Yvon) fitted with a 450 W Xenon lamp. The absolute Quantum Yield values were measured on a Quantaurus-QY Absolute PL Quantum Yield spectrometer C11347. The ^1H NMR spectrum was recorded at room temperature on a Bruker Avance I - 300 MHz spectrometer. The sample was dissolved in DMSO-d_6. Chemical shifts (δ) are reported in parts per million and were referenced to the residual signal of the solvent (δ = 2.50 ppm). Scanning Electron microscopy (SEM) images were obtained using a JEOL 6700F microscope equipped with a field emission gun operating at 3.0 kV in the secondary electron imaging (SEI) mode. C, H, and N elemental analyses were carried out at the Service Commun d'Analyses of the University of Strasbourg. The metal content was determined from the weight of the residues after ThermoGravimetric Analyses up to 900°C, having checked by PXRD that the residues were Co_3O_4 and ZnO for the Co and Zn hybrids respectively.

Thermo-Gravimetric Analyses (TGA) / Differential Thermal Analysis (DTA) was performed on a TA Instrument SDT600 apparatus in Pt crucibles under air atmosphere with a heating rate of 5°C/min. The magnetic studies were carried out with a SQUID magnetometer (Quantum Design MPMS3) covering the temperature and field ranges 2–300 K and ±7 T respectively. Magnetization versus field measurements at room temperature confirms the absence of ferromagnetic impurities. Data were corrected for the sample holder, and diamagnetism was estimated from Pascal constants.

All reactants and solvents were used as purchased without any further purification.

N-Sali-COOH,[61] $Co_5(OH)_8(OAc)_2 \cdot 2H_2O$,[62] $Co_5(OH)_8(DSO_3)_2 \cdot 2H_2O$,[62] $Zn_5(OH)_8(DSO_4)_2 \cdot 2H_2O$ [63] where $OAc^- = CH_3COO^-$, $DSO_3^- = C_{12}H_{25}SO_3^-$ and $DSO_4^- = C_{12}H_{25}SO_4^-$ were synthesized following already published procedures.

N-Sali-$SO_3 \cdot HNEt_3$: *N*-Sali-$SO_3 \cdot HNEt_3$ was synthesized as the triethylammonium salt of sulfonate group. 1.73 g (10 mmol) of *p*-sulfanilic acid was added to 50 mL of MeOH in a round bottom flask. To this solution was then added 1.4 mL (10 mmol) of triethylamine. The reaction mixture was stirred at 60°C for one hour. 1.04 mL (10 mmol) of salicylaldehyde were then added to the reaction mixture. The resulting yellow color reaction mixture was stirred for 4 h at 60°C. The solvent was evaporated on a rotary evaporator under reduced pressure. The resulting yellow powder was then recrystallized in hot MeOH to obtain crystalline triethylammonium salt of *N*-Sali-$SO_3 \cdot HNEt_3$. Yield: 74.86% (2.83 g). Major FT-IR stretching/vibrational bands (ATR, cm^{-1}) : 2979(w), 2883(w), 2712(w), 1621 (m) 1592(w), 1573(m), 1475(m), 1455(m), 1390(m), 1283(m), 1182(s), 1118(s), 1026(s), 854(s). ^1H NMR [300 MHz, DMSO-d_6, δ (ppm)] : 13.01 (s, 1H), 8.93 (s, 1H), 7.64 (d, J = 8.4 Hz, 2H), 7.42 (d, J = 8.4 Hz, 2H),

7.36 (t, *J* = 8.4 Hz, 1H), 7.24 (d, *J* = 8.7 Hz, 1H), 6.97 (t, *J* = 8.1 Hz, 1H), 6.43 (d, *J* = 8.4 Hz, 1H), 3.09 (d, *J* = 6.6 Hz, 6H), 1.17 (t, *J* = 7.2 Hz, 9H)

Co-*N*-Sali-R (R = -COO, -SO_3): 1.11 mmol of *N*-Sali-R (R = -COOH, -$SO_3 \cdot HNEt_3$) was added to 40 mL of EtOH. To this solution was added 0.28 mL (2.0 mmol) of Et_3N. The clear yellow solution was bubbled with argon at 60°C for 20 min. To this solution was then added a suspension of 0.215 g (0.222 mmol) of $Co_5(OH)_8(DSO_3)_2 \cdot 2H_2O$ in 15 mL EtOH. The reaction mixture was stirred for 1 h at 60 °C under argon. The reaction mixture was cooled down, filtered and washed three times with EtOH to lead to a light green color compound.

Co-*N*-Sali-COO: 0.164 g. Major FT-IR stretching/vibrational bands (ATR, cm^{-1}) : 1595(s), 1531(s), 1380(s), 1278(m), 1174(m), 1151(w), 1099(w), 1042(w), 1011(w), 911(w), 857(w), 822(w), 754(m), 683(w), 515(m). Anal. Calcd for $Co_5(OH)_{8.68}$(*N*-Sali-COO)$_{1.3}(DSO_3)_{0.02} \cdot 5H_2O$ (M = 849.7 $g \cdot mol^{-1}$) (%): C, 26.07; H, 3.82; N, 2.14; Co, 34.68; Found (%) : C, 25.99; H, 3.77; N, 2.24; Co, 33.87.

Co-*N*-Sali-SO_3: 0.152g. Major FT-IR stretching/vibrational bands (ATR, cm^{-1}) 1607(m), 1531(w), 1463(w), 1439(w), 1380(w), 1174(s), 1122(s), 1031(s), 1007(s), 834(w), 758(w), 713(w), 693(w), 555(m). Anal. Calcd for $Co_5(OH)_{8.98}$(*N*-Sali-SO_3)$(DSO_3)_{0.02} \cdot 4H_2O$ (M = 800.7 $g \cdot mol^{-1}$) (%): C, 19.86; H, 3.46; N, 1.75; Co, 36.80; Found (%): C, 19.69; H, 3.82; N, 1.59; Co, 36.50.

Zn-*N*-Sali-R (R = -COO, -SO_3): 1.0 mmol of *N*-Sali-R (R = -COOH, -$SO_3 \cdot HNEt_3$) was added to 40 mL of EtOH. To this solution was added 0.28 mL (2.0 mmol) of Et_3N. The clear yellow solution was bubbled with argon at 60°C for 20 min. To this solution was then added a suspension of 0.191 g (0.2 mmol) of $Zn_5(OH)_8(DSO_4)_2 \cdot 2H_2O$ in 15 mL EtOH. The reaction mixture was stirred

for 24 hours at 45°C under argon. The reaction mixture was cooled down, filtered and washed three times with EtOH to lead to a yellow color compound.

Zn-*N*-Sali-COO: 0.09 g. Major FT-IR stretching/vibrational bands (ATR, cm^{-1}) 1595(s), 1542(s), 1383(s), 1279(m), 1173(m), 1150(w), 1103(w), 1031(w), 1011(w), 911(w), 858(w), 825(w), 750(m), 684(w), 519(m). Anal. Calcd for $Zn_5(OH)_8$(*N*-Sali-COO)$_{1.9}(DSO_4)_{0.1}\cdot 3H_2O$ (M = 1000.0 $g\cdot mol^{-1}$) (%): C, 33.39; H, 3.58; N, 2.66; Zn, 32.69; Found (%): C, 34.11; H, 3.62; N, 2.53; Zn, 33.76.

Zn-*N*-Sali-SO_3: 0.136 g. Major FTIR stretching/vibrational bands (ATR, cm^{-1}) 1607(m), 1533(w), 1463(w), 1439(w), 1388(w), 1175(s), 1122(s), 1031(s), 1005(s), 836(w), 758(w), 714(w), 693(w), 570(m). Anal. Calcd for $Zn_5(OH)_{8.82}$(*N*-Sali-SO_3)$_{1.17}(DSO_4)_{0.01}\cdot 4H_2O$ (M = 874.9 $g\cdot mol^{-1}$); Calculated (%): C, 21.05; H, 3.31; N, 1.87; Zn, 37.37; Found (%): C, 21.5; H, 3.13; N, 2.15; Zn, 38.40.

RESULT AND DISCUSSION

Over the years, various methods have been used for the synthesis of functionalized LSHs including hydrothermal reaction,[44] confined condensation,[64] and even post-synthetic modification[65] methods. However, the most widely and versatile strategy is the insertion-grafting reaction by ion exchange.[7] In insertion grafting reaction, the anions present in the originally synthesized LSH are replaced by the functional anions which must bear either a carboxylate, sulfonate, sulfate or phosphonate groups as grafting groups for the anion exchange reaction to take place. In case of Co-LSH and Cu-LSH which are originally synthesized with acetate anions in the interlamellar space, a pre-intercalation strategy has proven to be very effective, especially for the insertion of large aromatic molecules such as azo dies, salen-type complexes and fluoren

derivatives.[43,47,49,50] In such pre-intercalation, the acetate anions are first replaced by large anions bearing long-alkyl chains, dodecyl sulfate or dodecyl sulfonate, using anion exchange reaction. The larger interlamellar spacing provided by the insertion of these anions, as well as the hydrophobic environment they create in the interlamellar space ease the subsequent ion-exchange by the desired molecules, that can be bulky, aromatic and/or fragile with respect to hydrolysis. For the insertion of *N*-Sali-R (R = SO_3^-, COO^-), we had to modify the second-step anion exchange reaction procedure. The standard procedure uses a mixed solvent EtOH/H_2O medium with the pH of the reaction mixture being adjusted to 8.0 - 9.0 using aqueous NaOH solution.[43] However, due to the sensitivity of *N*-salicylidene aniline molecules to hydrolysis,[66,67] we avoided the use of water as solvent (although no precaution was necessary to dry solvents and reactants, or to protect the products from air moisture). Therefore, the insertion of *N*-Sali-R was performed in EtOH, without addition of water at 60°C under inert atmosphere. Triethylamine (Et_3N) was added to the reaction mixture to the necessary basic conditions. The addition of Et_3N also enhanced the solubility of the *N*-Sali-R anions in EtOH, which otherwise would require large quantity of EtOH to be completely soluble. Finally, *N*-Sali-R has to be in large excess with respect to the dodecylsulfonate or dodecylsulfate to be exchanged. After filtration, three thorough washings with ethanol are required, in order to ensure the complete removal of the unreacted *N*-Sali-R anions, dodecylsulfonate or dodecylsulfate which have been exchanged (in the form of a triethylammonium salt) and unreacted trimethylamine. The anion exchange reaction in Co-LSH proceeded quite rapidly as it required only an hour for the complete exchange. To synthesize Zn-*N*-Sali-R (R = SO_3^-, COO^-), the anion exchange was performed from $Zn_5(OH)_8(DSO_4)_2 \cdot 2H_2O$ (where DSO_4 is dodecylsulfate) which was synthesized using a co-precipitation method.[63] The exchange did not proceed as straightforwardly as it did in case of Co-LSH. Indeed, in order to

obtain the single-phase Zn-*N*-Sali-R hybrid materials the reaction time had to be increased to 24 hours. This is in line with the already reported difficulties to perform ion-exchange reactions in Zn-LSH with large molecules.[68,69]

The structural characteristics of the synthesized hybrid materials were obtained using FT-IR spectroscopy and powder X-ray diffraction. The FT-IR spectra for the synthesized hybrid LSHs are given in Figure 1. The IR spectra of Co-*N*-Sali-COO and Zn-*N*-Sali-COO are very similar. For both these hybrid LSHs, intense peaks were observed at 1595 and 1380 cm^{-1} which corresponds to the asymmetrical and symmetrical stretching bands of the carboxylate group respectively. The difference $\Delta\nu = \nu_{asym} - \nu_{sym}$ equals 215 cm^{-1}. This relatively large value suggests a monodentate coordination mode of the carboxylate moiety.[70–74] In addition, a shoulder at *ca.* 1605 cm^{-1} and a strong band at 1539(Zn) and 1531(Co) cm^{-1} can be attributed to C=O and N=C vibrational bands of *N*-Sali-COO, thus indicating the successful insertion of *N*-Sali-COO into Co-LSH and Zn-LSH. The small peaks at 2921 and 2853 cm^{-1} correspond to the alkyl chain of dodecyl sulfonate/sulfate which suggests the presence of traces of the pre-intercalated anions.

The IR spectra of Co-*N*-Sali-SO_3 and Zn-*N*-Sali-SO_3 are also very similar. They show intense vibrational bands of the sulfonate group at around 1179(Zn), 1174(Co), 1032 and 835 cm^{-1}. As for the carboxylate analogues, C=O and N=C vibrational bands of *N*-Sali-SO_3 can be identified at 1615(Zn), 1607(Co) and 1535(Zn) and 1531(Co) cm^{-1}. Traces of remaining dodecyl sulfonate/sulfate are responsible for peaks at 2921 and 2853 cm^{-1}.

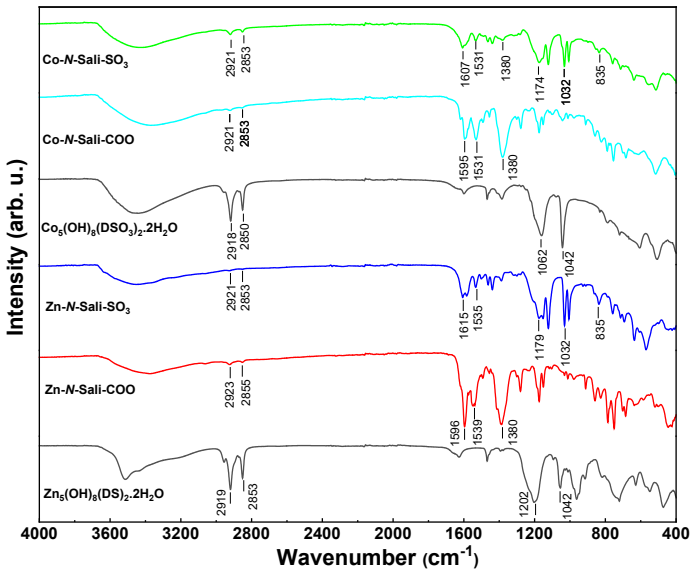

Figure 1. FT-IR spectra of the synthesized hybrid LSHs and of the starting phases

The PXRD patterns of the synthesized hybrids are shown in Figure 2. Profile matching (Le Bail) refinements of the XRD experimental diffractograms of Co-*N*-Sali-COO, Co-*N*-Sali-SO_3 and of the starting materials $Zn_5(OH)_8(DSO_4)_2 \cdot 2H_2O$ and $Co_5(OH)_8(DSO_3)_2 \cdot 2H_2O$ were performed using the Fullprof software[75] and using the structure of the archetypical compound in this family, $Zn_5(OH)_8(NO_3)_2$,[36] as a base for the space group and basal parameters determination (Figure S1). The crystallinity along the *c* axis of the Zn-*N*-Sali-R hybrid compounds is poorer than the one of the Co analogues, despite many attempts to optimize it. This very large distribution of the interlayer distances prevents a reasonable profile matching. The interlayer distance retained in the following for the Zn-*N*-Sali-R hybrid compounds is determined from the position of the maximum of the first low angle peak. All the PXRD patterns show intense *00l* diffraction peaks, up to at least the fourth harmonic which indicates the stacking periodicity of the inorganic layers and marks the layered structure of the synthesized hybrid materials. The absence of *00l* diffraction peaks coming from the starting compounds and the marked change in the positions of the *00l* diffraction peaks

confirm the formation of single-phased Co-*N*-Sali-R and Zn-*N*-Sali-R. In the case of Zn-*N*-Sali-R though, the broadness of the *00l* peaks indicates a relatively higher disorder with an important distribution of interlayer spacings. The 2θ positions of the *00l* diffraction peaks determine the basal spacing for each compound of 2.161(4), 2.155(1), 2.9(1) and 2.2(1) nm for Co-*N*-Sali-COO, Co-*N*-Sali-SO_3, Zn-*N*-Sali-COO and Zn-*N*-Sali-SO_3 respectively.

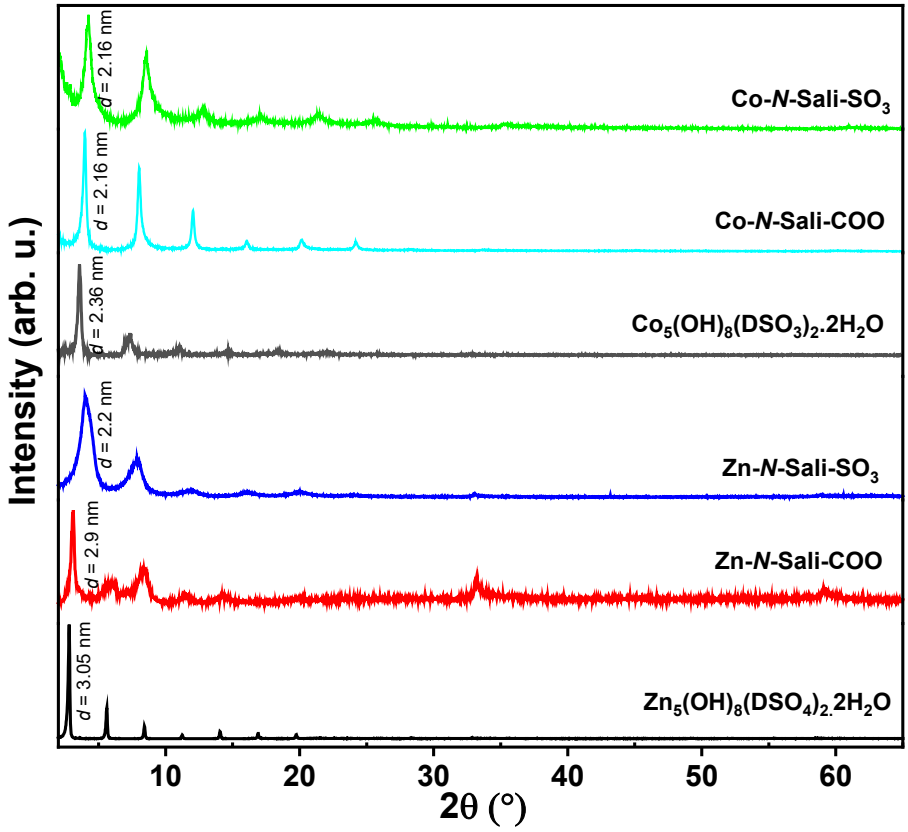

Figure 2. PXRD patterns of the synthesized hybrid Co-*N*-Sali-COO, Co-*N*-Sali-SO_3, Zn-*N*-Sali-COO and Zn-*N*-Sali-SO_3 and of the starting materials $Zn_5(OH)_8(DSO_4)_2 \cdot 2H_2O$ and $Co_5(OH)_8(DSO_3)_2 \cdot 2H_2O$.

The interlamellar distances for the two cobalt hybrids Co-*N*-Sali-COO and Co-*N*-Sali-SO_3 are very close, 2.161(4) and 2.155(1) nm respectively, indicating a similar grafting and arrangement

of the molecules in the interlamellar space. On the contrary the difference in the basal spacings of Zn-*N*-Sali-COO and Zn-*N*-Sali-SO_3, 2.9(1) and 2.2(1) nm respectively, is quite large. This can be explained by the larger amount of remaining dodecyl sulfate in Zn-*N*-Sali-COO than in Zn-*N*-Sali-SO_3 (0.1 and 0.01 *per* formula unit respectively), which would tend to further increase the interlamellar distance as it has been shown in the case of LDH.[76] Another explanation, considering the quite small amount of residual dodecyl sulfate in Zn-*N*-Sali-COO, is the different grafting of the carboxylate and sulfonate derivatives of *N*-salicylidene aniline. Indeed it has already been shown that carboxylate ligands graft on the apical position of Zn tetrahedra in Zn-LSH,[77] whereas sulfate interact on the side of the Zn tetrahedra,[78] likely leading to different angles between the inserted molecule and the inorganic layers.

Considering an approximate length of *ca.* 1.3 nm for the planar *N*-Sali-R molecules[54,79], a thickness of the inorganic nanosheets of *ca.* 0.73 nm,[29,78] the experimental basal spacings are consistent with a double layer arrangement of the *N*-Sali-R molecules in-between inorganic layers, with partial inter-digitation.[43]

The SEM (scanning electron microscope) images (Figure S2) for all the hybrids show a micro-platelet morphology, typical of hybrid LSH, in line with their layered structure. The composition analysis by EDX (cartography of a 10^4 mm^2 area along with several 1 mm^2 spot analyses) underlines the homogeneity of the compounds.

The formula of all the compounds was determined using elemental (C, H, N), and Thermo Gravimetric Analyses (TGA) (see Experimental Section): $Co_5(OH)_{8.68}$(*N*-Sali-COO)$_{1.3}(DSO_3)_{0.02}\cdot 5H_2O$ (Co-*N*-Sali-COO), $Co_5(OH)_{8.98}$(*N*-Sali-SO_3)$(DSO_3)_{0.02}\cdot 4H_2O$ (Co-*N*-Sali-SO_3), $Zn_5(OH)_8$(*N*-Sali-COO)$_{1.9}(DSO_4)_{0.1}\cdot 3H_2O$ (Zn-*N*-Sali-COO) and $Zn_5(OH)_{8.82}$(*N*-Sali-SO_3)$_{1.17}(DSO_4)_{0.01}\cdot 4H_2O$ (Zn-*N*-Sali-SO_3). From these formula, it appears that the anion exchange

proceeds more efficiently when the organic anions bear a carboxylate group than when they bear a sulfonate group.

The TGA/DTA were obtained under air atmosphere with a heating rate of 5°C/min (Figure 3). The TGA indicate a multi-step decomposition of the synthesized hybrids. The first event, between 25°C and 150°C for Co-*N*-Sali-R and up to 220°C for Zn-*N*-Sali-R is slightly endothermic and corresponds to the release of water molecules adsorbed at the surface of the crystallites or present in the interlayer space. The quantity of water determined from TGA curves are in good accordance with the formula determined from elemental analyses (TGA(Anal) (%): 8.6(10.6), 8.3(9.0), 10.8(5.4), 12.6(8.3) for Co-*N*-Sali-COO, Co-*N*-Sali-SO_3, Zn-*N*-Sali-COO, and Zn-*N*-Sali-SO_3 respectively. For Co-*N*-Sali-R, a second region between 200°C and 400°C consists of a series exothermic events including a strongly exothermic one which can be attributed to the thermal decomposition of the intercalated *N*-Sali-R molecules and dehydroxylation of the hydroxide layers.[80,81] Similar exothermic events are observed for Zn-*N*-Sali-R hybrids but at a much higher temperature, which indicates that the Zn-LSH hybrids provide a much higher thermal stability to the intercalated organic compounds than their cobalt counterparts. It is noteworthy here that the pristine *N*-Sali-R molecules decompose in the range 200-290°C (Figure S3). Finally, LSHs inserted with *N*-Sali-SO_3 have a slightly higher thermal stability and decompose more gradually than the LSHs inserted with *N*-Sali-COO, in line with what has already been observed in other LSHs[43] and in LDHs.[82,83]

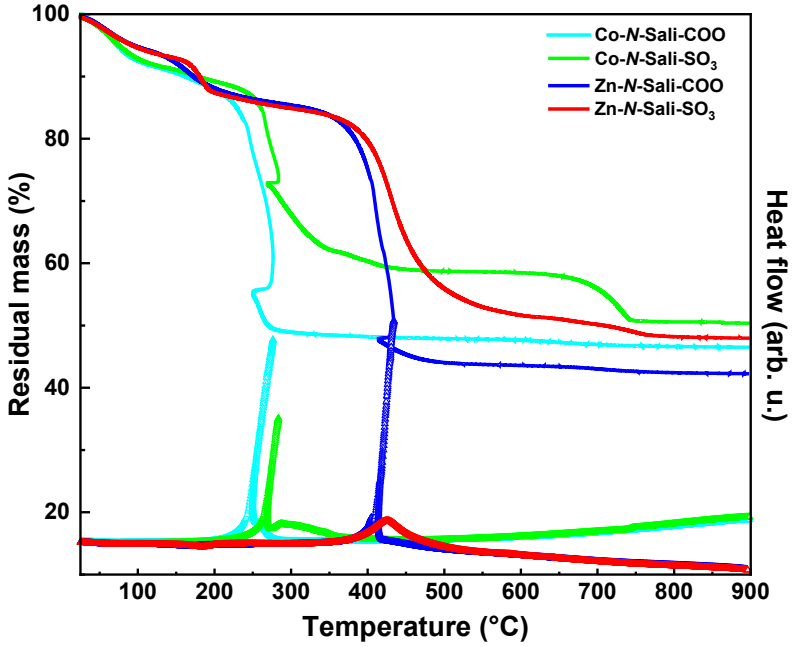

Figure 3. TGA (full lines) and DTA (open triangles) for the synthesized hybrids Co-*N*-Sali-R and Zn-*N*-Sali-R. The folded curves are due to the temperature regulation process of the apparatus during a strongly exothermic event.

At high temperature, above 700°C, all compounds get oxidized to their metal oxide forms, Co_3O_4 and ZnO for the Co and Zn hybrids respectively. The metal content of the LSHs were deduced from the metal oxide residue left at 900°C (see experimental section).

The UV-Vis. diffuse reflectance (DRS) (Figure 4) were recorded on pure powder samples without diluting them in any film or matrix because matrix effects can influence the enol-keto population of *N*-salicylidene aniline molecules which in turn would affect the optical properties of the synthesized samples.[84–86] The DRS spectra of the pristine *N*-Sali-R clearly show that both the enol and *cis*-keto forms co-exist in the solid state at room temperature. Yet, the population of the

cis-keto form is more important in *N*-Sali-COOH than in *N*-Sali-$SO_3 \cdot HNEt_3$ where the enol form dominates.[54,87,88]

As for the hybrid materials, the relative population of the enol and *cis*-keto is more difficult to infer from the DRS spectra as the absorption bands overlap with the expected metal to ligand charge transfer bands. Nevertheless, the spectra suggest that still both enol and *cis*-keto forms co-exist in Co-*N*-Sali-R as well as in Zn-*N*-Sali-R LSHs.

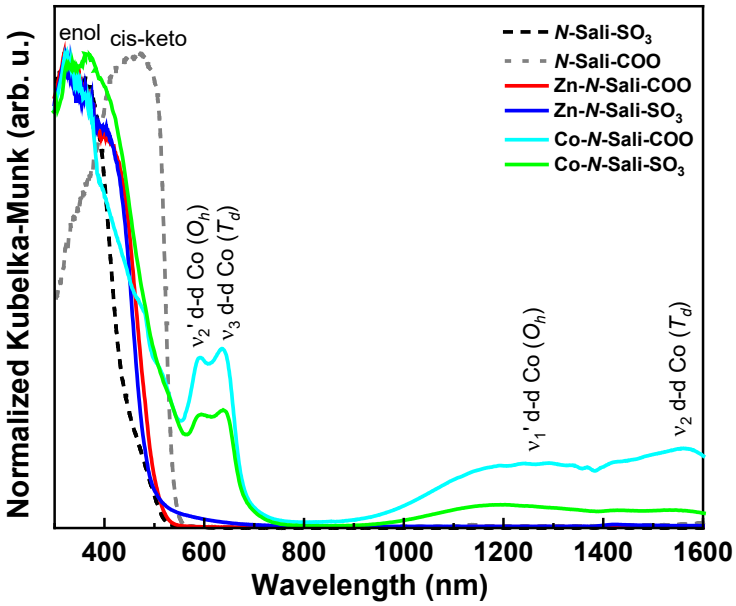

Figure 4. DRS spectra at room temperature of the synthesized Co-*N*-Sali-R and Zn-*N*-Sali-R LSHs and of the pristine organic compounds *N*-Sali-R (in dashed curve). The DRS spectra of the pristine materials $Zn_5(OH)_8(DSO_4)_2$ and $Co_5(OH)_8(DSO_3)_2$ are presented for comparison in Figure S4.

In addition, the Co-*N*-Sali-R hybrids present characteristic, and identical, absorption bands in the NIR and visible regions, around 1560 (ν_2) and 1250 nm (ν_1') and at 636 (ν_3) and 590 nm (ν_2'), with a shoulder around 500 nm (ν_3'). ν_2 and ν_3 can be attributed to the $^4A_2(F) \rightarrow {}^4T_1(F)$ and

$^4A_2(F) \rightarrow {}^4T_1(P)$ transitions of Co(II) in T_d environment respectively, whereas ν_1', ν_2' and ν_3' and can be attributed to the $^4T_{1g}(F) \rightarrow {}^4T_{2g}(F)$, $^4T_{1g}(F) \rightarrow {}^4A_{2g}(F)$ and $^4T_{1g}(F) \rightarrow {}^4T_{1g}(P)$ transitions of HS Co(II) in O_h environment respectively.[45,89] The first expected transition of Co(II) in *Td* environment, $^4A_2(F) \rightarrow {}^4T_2(F)$ is at a too low energy to be observed here (typically 2300-3500 nm). The $^4T_{1g}(F) \rightarrow {}^4A_{2g}(F)$ transition (ν_2') is formally a two electron transition, so generally not-observed. Yet it may be observed in the 12000-18000 cm^{-1} (555-833 nm) and safely attributed provided the ratio E_2'/E_1' is in the range 2.1-2.2.[89] From these spectra and the Tanabe-Sugano diagrams, the D_q and Racah's repulsion parameter B can be evaluated[90,91], providing $D_q \sim 910$ cm^{-1} and $B \sim 880$ cm^{-1} for Co(II) in O_h environment and $D_q \sim 370$ cm^{-1} and $B \sim 740$ cm^{-1} for Co(II) in T_d environment. The nephelauxetic parameter β is evaluated at 0.91 and 0.76 for Co(II) in *Oh* and T_d environment respectively, considering $B_{isolated} = 971$ cm^{-1} for Co(II).[89] The lower value of β for the Co(II) in T_d environment is in accordance with a higher degree of covalency due to the grafting of the carboxylate or sulfonate moieties.

The photochemical processes that occur in pristine *N*-salicylidene anilines are depicted in Scheme 3. The UV irradiation converts the enol conformer to the *trans*-keto form through a meta-stable *cis*-keto* state, whereas the irradiation with blue light causes the *cis*-keto to *trans*-keto photo-isomerization.[53,54,88]

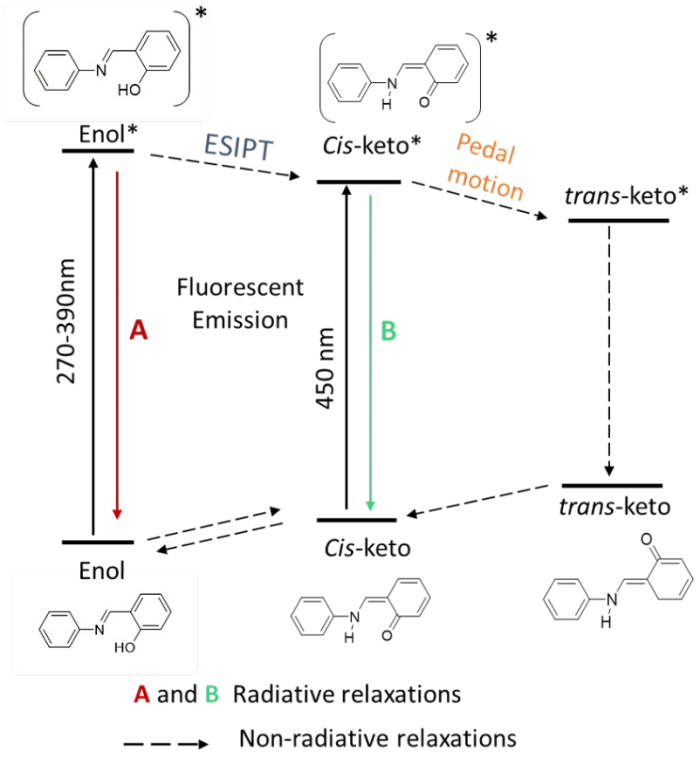

Scheme 3. Photochemical process pathways for *N*-salicylidene anilines upon irradiation. ESIPT stands for Excited State Intra-molecular Proton Transfer.

The irradiation with UV light, and blue light (450 nm) showed no visible photochromism in Co-*N*-Sali-R and the color of the LSHs remained intense green. However, in case of Co-*N*-Sali-R, the *cis*-keto bands are not well resolved and overlap with the *d-d* transition bands of Co(II) ions which makes it difficult to the infer the presence of any *trans*-keto form in Co-*N*-Sali-R.

Owing to the fact that Zn-LSH and Co-LSH possess a similar structure, the photochemical behavior of *N*-Sali-R in Co-*N*-Sali-R can be explained on the basis of Zn-*N*-Sali-R. To probe the possible formation of the *trans*-keto form, the Zn-LSHs have the strong advantage not to present any absorption bands in the visible region which might interfere with the *cis*-keto bands. Actually, no visible change in color was observed in Zn-*N*-Sali-R upon irradiation with the UV light, and

blue light (450 nm). The DRS spectra of the Zn-*N*-Sali-R remained the same after irradiation, further confirming the absence of any *trans*-keto form and photoisomerization.

The reason for the absence of *cis-trans* photoisomerization in the synthesized hybrid LSHs can be explained by the arrangement of the *N*-Sali-R molecules in-between the interlayers. Indeed, the *cis-trans* photoisomerization in *N*-salicylidene anilines takes place through a pedal motion.[53] To ensure that the pedal motion is not hindered in the lattice, certain requirements should be met for this pedal motion to take place in the solid state. These requirements can be narrowed down to two factors which include: *(i)* the large free available space in the lattice, *(ii)* no or weak intermolecular interactions.[53,92] In the present case, interdigitation between the *N*-Sali-R molecules might reduce the free space available for the pedal motion to take place. Furthermore, the water molecules present in the interlayer spacing can form hydrogen bonds with the *N*-Sali-R molecules which would also contribute in restricting the pedal motion, thus explaining the absence of *cis-trans* photoisomerization in the synthesized hybrid LSHs.

In order to probe the first part of the photochemical process described in Scheme 3, *i.e.* the Excited State Intra-molecular Proton Transfer (ESIPT), solid state emission spectroscopy was carried out, using an excitation wavelength λ_{exc} = 350 nm, which falls in the absorption band of the enol form of *N*-Sali-R (Figure 4). ESIPT is the intra-molecular proton transfer which takes place between the excited enol* and *cis*-keto* states (Scheme 3). In *N*-salicylidene anilines in the solid state, the timescale of this ESIPT process is a few hundred picoseconds.[93] The relaxation process from *cis*-keto* to *cis*-keto, pathway B in Scheme 3, is a radiative relaxation and the *N*-salicylidene anilines usually emit large Stokes-shifted fluorescent through pathway B.[88,92,94] In the absence of ESIPT process, the excited state enol* relaxes back to the en5ol ground state which is

also a radiative relaxation, marked as pathway A in Scheme 3. The emission spectra of the synthesized LSHs and of the pristine *N*-Sali-R molecules are shown in Figure 5. The pristine LSH hosts, $Zn_5(OH)_8(DSO_4)_2 \cdot 2H_2O$ and $Co_5(OH)_8(DSO_3)_2 \cdot 2H_2O$ do not emit light in these conditions. All the compounds give quite broad emission bands, which is a common observation for *N*-salicylidene anilines in solid-state and which can be ascribed to conformations of *N*-Sali-R, whose ground and excited state energy levels lie close to each other.[84,86]

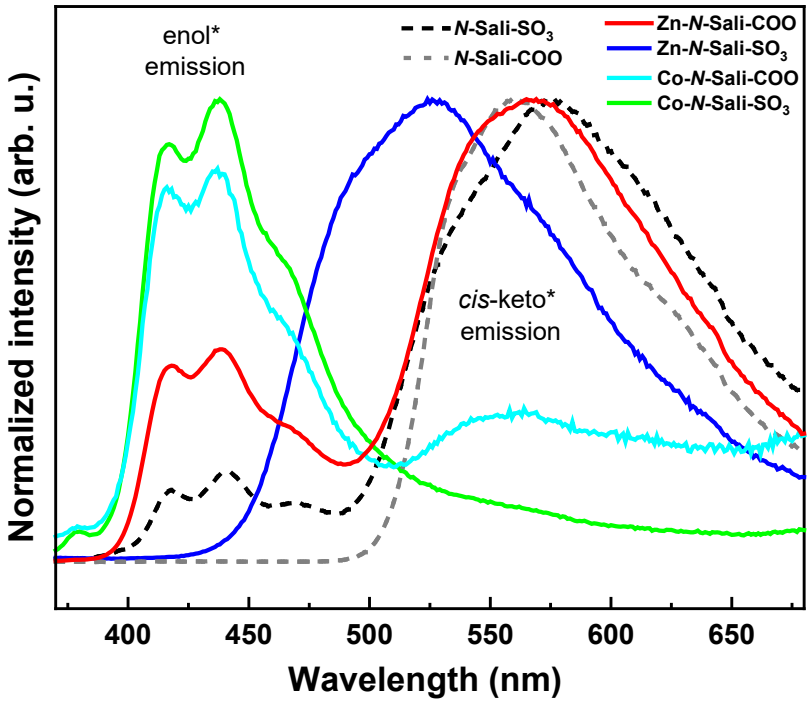

Figure 5. Room temperature emission spectra (λ_{exc} = 350 nm) of Co-*N*-Sali-R and Zn-*N*-Sali-R LSHs and of pristine organic compounds *N*-Sali-R.

Both organic compounds, *N*-Sali-R show a broad emission which spread from 490 to 680 nm which is attributed to the *cis*-keto* emission.[88] The wavelength for maximum *cis*-keto* emission ($\lambda_{max\text{-}cis*}$) for *N*-Sali-COOH and *N*-Sali-$SO_3 \cdot HNEt_3$ are 560 nm and 575 nm respectively. *N*-Sali-

COOH presents another emission ranging from 390 to 480 nm, attributed to the enol* emission.[88] The enol* emission band is constituted by two poorly resolved contributions having $\lambda_{max\text{-}enol*}$ of 417 and 438 nm which suggests the presence of two different enol* conformations.[88] Interestingly, no enol* emission was seen in the spectrum of *N*-Sali-SO_3·$HNEt_3$, indicating that all the enol conformers in *N*-Sali-SO_3·$HNEt_3$ have high reactivity towards ESIPT. The emission spectrum of Zn-*N*-Sali-COO is slightly different and shows contributions from *cis*-keto* as well as from enol* emissions. This indicates that the reactivity of *N*-Sali-COO enol conformers towards ESIPT decreases when inserted inside Zn-LSH. The $\lambda_{max\text{-}cis*}$ in the hybrid is the same as for the parent organic molecule and Zn-*N*-Sali-COO presents yellow luminescence (Figure 6). On the contrary, Zn-*N*-Sali-SO_3 gives only the *cis*-keto* emission band which ranges from 425 to 680 nm with a $\lambda_{max\text{-}cis*}$ of 525 nm. This 50 nm hypsochromic shift compared to the parent molecule in the case of the sulfonate derivative indicates that the modification of the chemical environment (here induced by the insertion of the molecule) which is well known to influence the photophysical properties of *N*-salicylidene anilines,[84–86] is more important than in the case of the carboxylate derivative (Figure 6). Just like for the pristine *N*-Sali-SO_3·$HNEt_3$, no enol* emission band was seen for Zn-*N*-Sali-SO_3, indicating that the high reactivity of the molecule towards ESIPT is preserved when inserted inside Zn-LSH. This reactivity toward ESIPT likely results from a combination of electronic factors (the higher electron density on the imine group which can be inferred in the case of Zn-*N*-Sali-SO_3 results in a higher reactivity towards ESIPT) and more generally of the specific environment of the molecule within the intermellar space of the host, such as steric hindrance and polarizability, which are known to influence the emission properties of *N*-salicylidene aniline.[88,95]

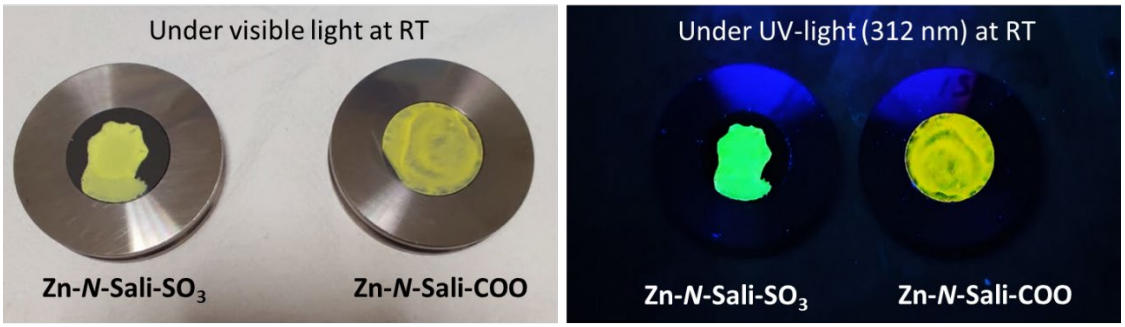

Figure 6. Photographs of Zn-*N*-Sali-R LSHs taken at room temperature under visible light (left) and UV light (right).

On the contrary, in case of Co-*N*-Sali-R, the enol* emission bands were found to be the dominating ones, suggesting that *N*-Sali-R lost most of their reactivity towards ESIPT when inserted inside Co-LSH. Even though a very broad contribution from *cis*-keto* emission, relatively low in intensity was also seen in both Co-*N*-Sali-R LSH, the luminescence in the visible range was not detected by the naked eye.

In addition to photochromism, *N*-salicylidene anilines exhibit temperature-induced keto-enol tautomerization which is mostly accompanied by thermochromism. The enol form (white) is favored at low temperatures whereas keto form (yellow) is predominant at higher temperatures. We thus probed the possible thermally induced keto-enol tautomerization of the intercalated *N*-Sali-R anions by monitoring the changes in the diffractograms of Co-*N*-Sali-R and Zn-*N*-Sali-R.

As inferred from the diffuse reflectance spectra, the enol and *cis*-keto forms were found to co-exist in the intercalated *N*-Sali-R at room temperature for all the synthesized LSHs. The diffractograms were measured with a temperature sequence of 25°C → -100°C → -180°C → 25°C → 60°C. We avoided further heating of the sample as it would also involve the changes in the

diffractograms related to evaporation of water molecules. The changes in the diffraction patterns of all the synthesized hybrids upon temperature variation are reported in Figure 7.

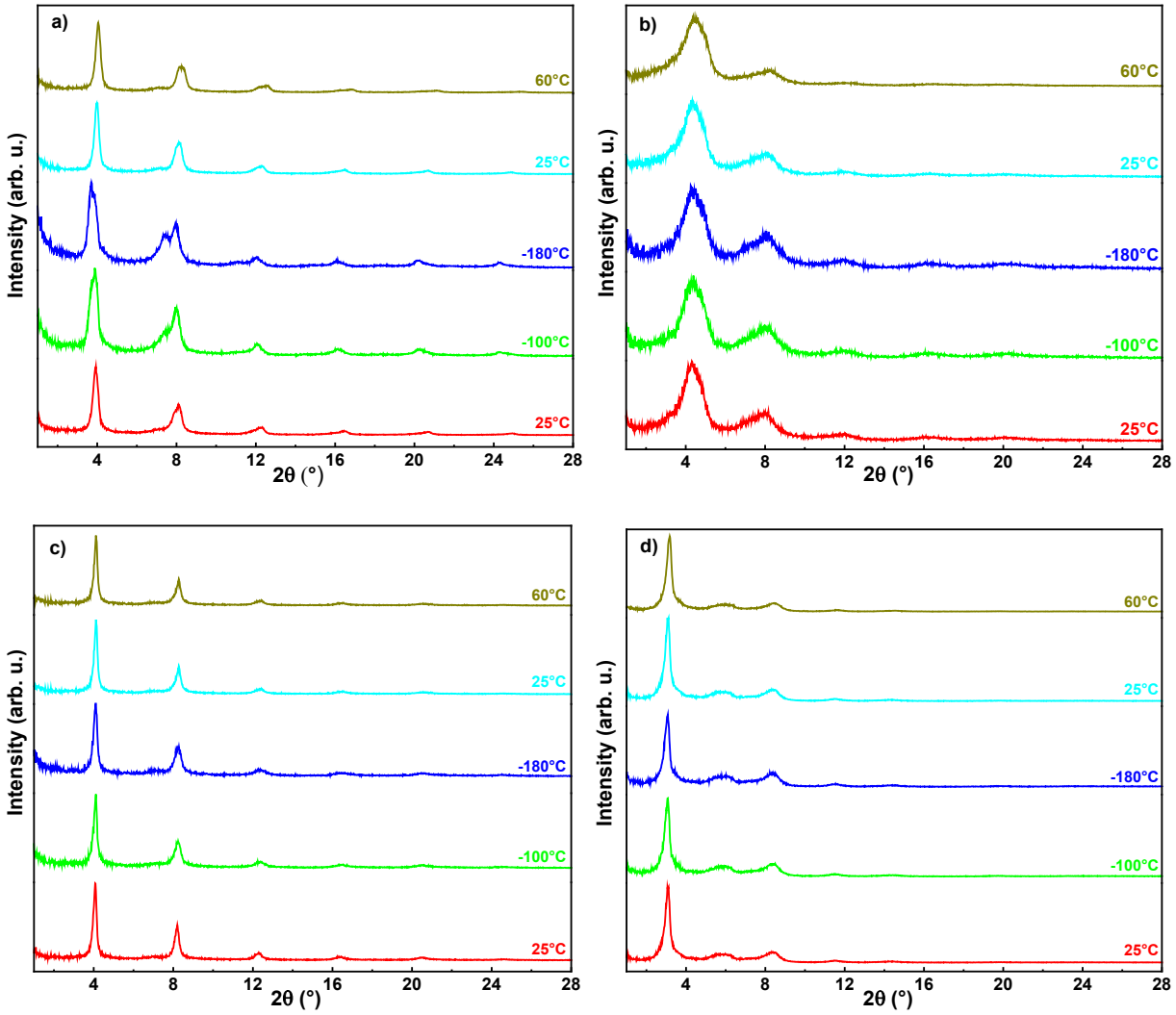

Figure 7. Temperature dependence of PXRD patterns for (a) Co-*N*-Sali-SO_3, (b) Zn-*N*-Sali-SO_3, (c) Co-*N*-Sali-COO, and (d) Zn-*N*-Sali-COO.

The most important changes upon were observed in the diffractogram of Co-*N*-Sali-SO_3. At 25°C, the basal spacing is $d_{25°C}$ = 2.155(1) nm, and the hybrid LSH appears as single phased. As the temperature is lowered to -100°C and further to -180°C, a new layered phase appears, with *00l*

harmonics at smaller angles with respect to the starting 25°C phase. This new phase presents a basal spacing of 2.368(8) nm at -100°C which further extends to 2.385(5) nm at -180°C. When the temperature increases back to 25°C and up to 60°C, the intensity of the peaks related to this new phase decreases considerably and the peaks broaden, which prevents the determination of the associated basal spacing. The emergence of a new phase can be attributed to the expected keto to enol tautomerization of *N*-Sali-SO_3 at low temperature. The presence of two phases (the original and the new ones) at -180°C indicates that not all keto conformers of *N*-Sali-SO_3 got converted to enol conformers upon decreasing the temperature. This behavior of partial tautomerization is commonly observed in *N*-salicylidene anilines where some conformers can get stabilized in the lattice either by solvent molecules or matrix effect.[96,97] Upon raising back the temperature, although the peaks related to the low temperature "enol phase" are far less intense, they can still be distinguished for the higher harmonics, indicating a not-complete reverse tautomerization. The temperature effects in Co-*N*-Sali-SO_3 can be summed up as: *(i)* enol and keto forms co-exist in equilibrium at 25 °C with *d*-spacing of 2.15 nm; *(ii)* lowering the temperature to -180°C perturbs the enol-keto equilibrium by favoring the enol form, which leads to the emergence of a new phase in the diffractogram with *d*-spacing of 2.40 nm at -180°C, meanwhile the *d*-spacing of the starting phase also increases, in a lower extent, to 2.19 nm at -180°C; *(iii)* raising the temperature to 60°C, keto forms gets more populated which leads to the disappearance of the phase which had emerged at low temperatures, and to the overall contraction of the *d*-spacing to 2.10 nm at 60°C.

The basal spacings of Co-*N*-Sali-COO and Zn-*N*-Sali-SO_3 remain almost unchanged upon decreasing the temperature from 25°C to -180°C (Figure 7b, c and d). Zn-*N*-Sali-COO present a noticeable evolution (-0.2 Å), yet very small and hardly significant given the broadness of the *00l* peaks. On the contrary, a more important evolution occurs upon heating, up to 60°C, with

variations of *d* of -0.5 Å for Co-*N*-Sali-SO_3 and Zn-*N*-Sali-SO_3 and -1.2 Å for Zn-*N*-Sali-COO. For Co-*N*-Sali-COO the evolution upon heating to 60°C is not significant (-0.1 Å). The evolution of the basal spacing of the four hybrid compounds as a function of temperature is reported in Figure 8.

To rationalize these results, a control experiment was performed to monitor the evolution of the basal spacing of $Zn_5(OH)_8(DSO_4)_2 \cdot 2H_2O$ in order to observe the effects of temperature on a non-thermo-responsive LSH with an interlamellar spacing of the same order of magnitude (Figure S5). Upon decreasing the temperature from 25°C to -180°C, the basal spacing decreases by 1.5 Å, and increasing the temperature from 25°C to 60°C leads to an increase of the basal spacing by *ca.* 0.3 Å. The evolution upon heating above room temperature is in line with what has been described by Demel *et al.* on the same compound (although in our case the basal spacing varies in a lesser extent and no staging phenomenon was evidenced),[78] or for instance on a CoAl-LDH functionalized by dodecylsulfate.[52] However, to our best of knowledge, the effect of lowering the temperature on basal spacing for $Zn_5(OH)_8(DSO_4)_2 \cdot 2H_2O$ or any other Zn(II) based LSH has never been reported. Here, in the case of a non-thermo-responsive molecule, our observations fit well with the hypothesis of compression and expansion of the layered structure as the temperature is lowered and raised, due to the temperature-induced rearrangement of the alkyl chains.

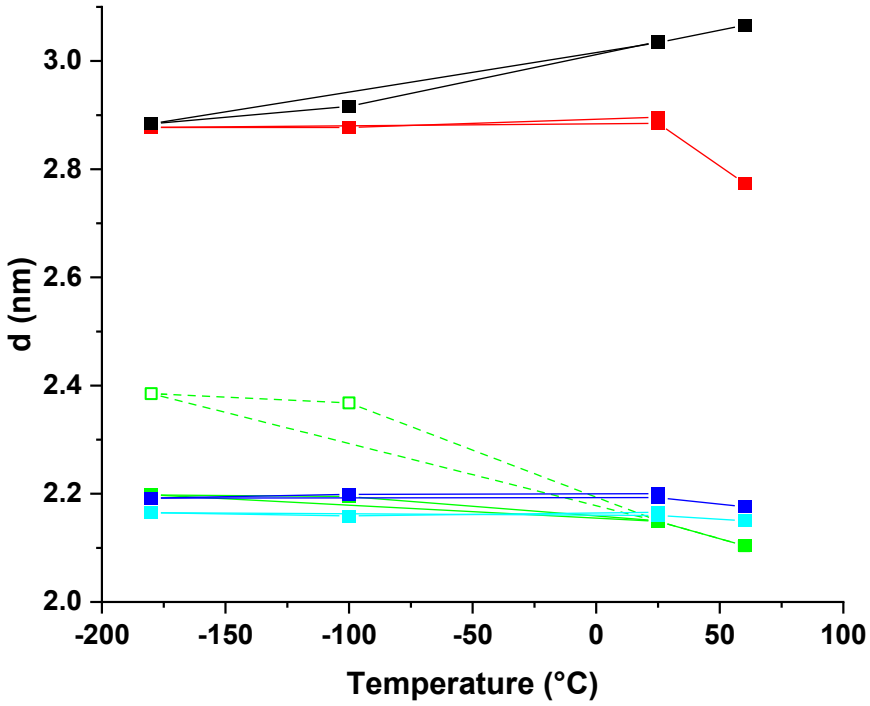

Figure 8. Evolution of the basal spacing (*d*) for Co-*N*-Sali-COO (cyan), Co-*N*-Sali-SO_3 (green), Zn-*N*-Sali-COO (red), Zn-*N*-Sali-SO_3 (blue) and $Zn_5(OH)_8(DSO_4)_2 \cdot 2H_2O$ (black) (Full squares are experimental points, full lines are just guide for the eye. The open squares and dotted line correspond to the low temperature phase which appears for Co-*N*-Sali-SO_3).

Therefore, in the case of hybrid LSHs functionalized with thermo-responsive molecules, two processes take place as the temperature is lowered(increased): *(i)* keto to enol (enol to keto) tautomerization, and *(ii)* thermally induced compression (expansion) of the layered structure. The tautomerization from keto (…C_1-NH-HC_2=C_1…) to enol (…C_1-N=C_2H-C_3…) form involves rearrangement of some bonds from single to double bond which changes the corresponding bond lengths and bond angles. From the reported crystal structures of *N*-salicylidene aniline type molecules, the difference in the lengths of *cis*-keto and enol forms is in the range 0.1 - 0.2 Å.[98–100] This small difference cannot explain alone the larger evolution observed upon decreasing the

temperature for Co-*N*-Sali-SO_3 (+0.7 Å) and upon increasing the temperature for Co-*N*-Sali-SO_3 and Zn-*N*-Sali-SO_3 (-0.5 Å), or Zn-*N*-Sali-COO (-1.2 Å). However, just like any other molecular rearrangement, the keto-enol tautomerization in *N*-salicylidene anilines also induces some strain in the lattice due to the change of bond lengths and bond angles, which may even induce thermosalient effect.[61,101] Therefore, one possible explanation for the evolution of the basal spacing of the layered hybrids described here is the combination of the molecular rearrangement induced by the keto-enol tautomerization and of the mere temperature induced dilatation/contraction of the layered structure evidenced in the case of $Zn_5(OH)_8(DSO_4)_2 \cdot 2H_2O$.

For Co-*N*-Sali-COO these two effects likely compensate both upon decreasing the temperature and upon increasing it. For Zn-*N*-Sali-COO and Zn-*N*-Sali-SO_3, the two effects compensate upon decreasing the temperature, but, upon increasing the temperature, the noticeable decrease of the interlamellar spacing (-1.2 Å and -0.5 Å respectively) indicate that the effect of the enol to keto tautomerization overcome the expansion effect. This is in line with the DRS results indicating that the enol form of *N*-Sali-R is the more populated one at room temperature for Zn-*N*-Sali-R. Therefore, the tautomerization of the residual keto form upon decreasing the temperature is likely to have little effect. On the contrary, the tautomerization of the large population of the enol form into the keto one upon increasing the temperature triggers the important reduction of the interlamellar spacing. Finally, in the case of Co-*N*-Sali-SO_3 the effect of the tautomerization (from keto to enol upon decreasing the temperature, and from enol to keto upon increasing it), largely overcome the dilatation/contraction of the layered structure.

The magnetic behaviours of the two Co-*N*-Sali-R hybrids were also investigated. The magnetic findings for the two compounds are similar, and in accordance with the typical behaviour of Co

(II) based LSH. Figure 9 represents the variation of the product of susceptibility by temperature (χT) as a function of temperature for the hybrid LSHs. The Curie constants deduced by using the Curie–Weiss law (not shown) are 13.4 and 14.0 emu·K·mol^{-1} for Co-*N*-Sali-COO and Co-*N*-Sali-SO_3 respectively, which agrees well with a mixture of tetrahedral and octahedral high spin Co(II) ions, with C_{tetra} = 2.2 to 2.8 emu·K·mol^{-1} for one Co(II) ion, and C_{octa} = 2.8 to 3.4 emu·K·mol^{-1} and five Co(II) ions *per* formula unit.[102] As the temperature is decreased from 300 K, a gradual decrease in χT product is observed down to a minimum (12.32 emu·K·mol^{-1} for Co-*N*-Sali-COO and 13.71 emu·K·mol^{-1} for Co-*N*-Sali-SO_3) at around 84 K. This slight decrease can be attributed to the spin–orbit coupling effect and/or antiferromagnetic interactions between the Co(II) moments. Cooling down further, a steep increase in the χT product is observed up to a maximum at 11.7 K (35.9 emu·K·mol^{-1}) for Co-*N*-Sali-COO and at 10.4 K (39.9 emu·K·mol^{-1}) for Co-*N*-Sali-SO_3. This steep increase is ascribed to the occurrence of long-range ferrimagnetic ordering.[40,43]

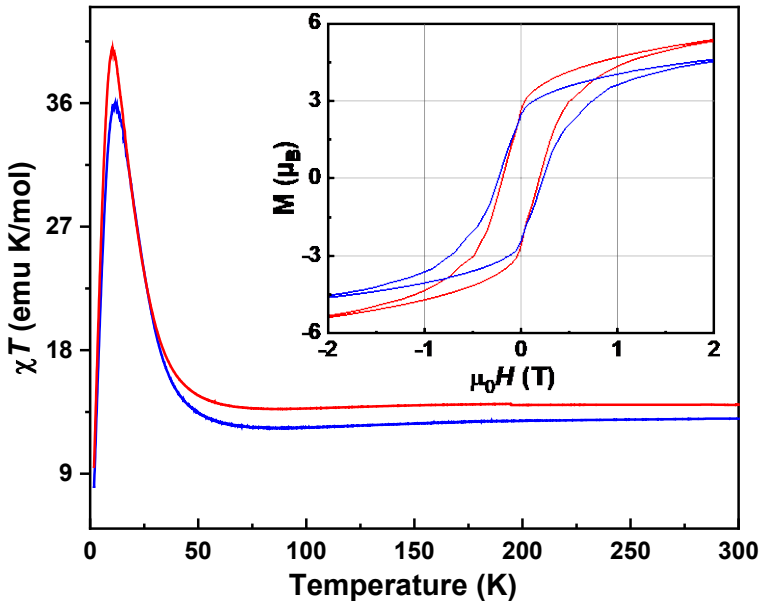

Figure 9. Magnetic behavior as χT *vs*. *T* plots of Co-*N*-Sali-COO (blue) and Co-*N*-Sali-SO_3 (red), under a magnetic dc field of 5000 Oe. Insert: zoom of the field dependence of the magnetization at T = 1.8 K (for full scale, see Figure S6).

The ordering temperature of the hybrid LSHs were determined using ac susceptibility measurements (Figure 10).

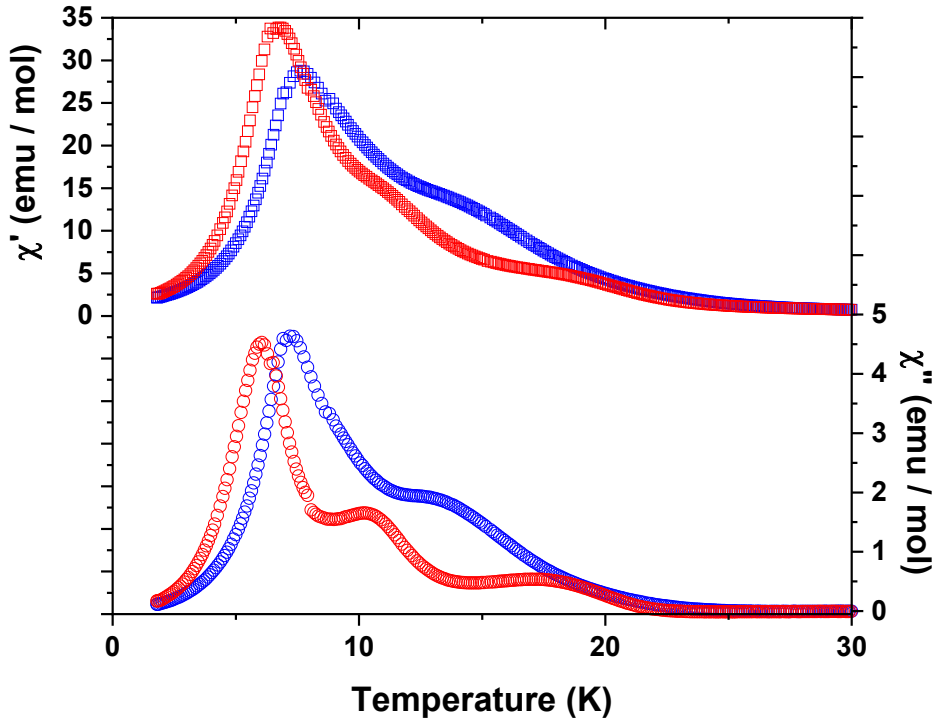

Figure 10. In phase (χ', open squares) and out of phase (χ", open circles) magnetic susceptibilities Co-*N*-Sali-COO (blue) and Co-*N*-Sali-SO_3 (red) (f = 970 Hz, H_{ac} = 2 Oe).

The maximum of the real part χ' provides T_N = 6.8 K and 7.7 K for Co-*N*-Sali-COO and Co-*N*-Sali-SO_3 respectively. The signal in χ' is accompanied by a signal in χ", confirming the ferrimagnetic nature of the magnetic ordering, due to antiferromagnetic superexchange interaction between Co(II) O_h and Co(II) T_d within the inorganic layers, and interlayer ferromagnetic coupling *via* dipolar interactions.[48,103] Both χ' and χ" for Co-*N*-Sali-R present several maxima and shoulders, none of these being frequency dependent, which is a typical behavior for layered hydroxide magnets and suggests a distribution of ordering temperatures, likely due to different microdomains.[25,34,41,45,47]

Finally, the ferromagnetic-type behavior of Co-*N*-Sali-COO and Co-*N*-Sali-SO_3 is confirmed by the magnetization *vs.* field curves at low temperature which show the presence of hysteresis loops

as shown in the inset of Figure 9 and in Figure S6. The values of coercive fields were found to be 240 mT for Co-*N*-Sali-COO and 200 mT for Co-*N*-Sali-SO_3. The low value of the moments at high field (M(7T) = 6.8 and 8.1 μB for Co-*N*-Sali-COO and Co-*N*-Sali-SO_3 respectively at 1.8 K) compared to the expected value for a total alignment of the moments (10–15 μ_B for five Co(II) ions) confirms a ferrimagnetic ordering.

CONCLUSION

The carboxylate and sulfonate derivatives of thermo and photoresponsive *N*-salicylidene aniline were successfully inserted into Co(II) and Zn(II) based LSHs resulting in four novel hybrid LSHs Co-*N*-Sali-COO, Co-*N*-Sali-SO_3, Zn-*N*-Sali-COO and Zn-*N*-Sali-SO_3. Owing to the sensitivity of *N*-salicylidene aniline towards hydrolysis, the standard anion exchange reaction procedure was successfully modified to synthesize these hybrids.

All synthesized hybrids present double organic layered type model in which *N*-Sali-R molecules are involved in intermolecular interactions, hindering the pedal movement of *N*-Sali-R molecules and resulting in the absence of *cis-trans* photoisomerization. Yet, the Zn analogs were found to be fluorescent when exposed to UV light, thanks to Excited State Intramolecular Proton Transfer mechanism, which leads to a strong emission from the *cis*-keto* to *cis*-keto relaxation. We showed on the contrary that when inserted in Co-LSH the *N*-Sali-R molecules have lower reactivity towards ESIPT process.

Temperature dependent PXRD was used to monitor the keto-enol tautomerization of the *N*-Sali-R molecules in LSHs. Upon decreasing the temperature down to -180°C, the keto to enol tautomerization was found to be very effective in the case of Co-*N*-Sali-SO_3, whereas upon

increasing the temperature up to 60°C, the enol to keto tautomerization was found to be very effective for all compounds except Co-*N*-Sali-COO.

The two Co-*N*-Sali-R compounds show the classical behavior of Co(II) based LSH exhibiting long range ferrimagnetic ordering at low temperature, with T_N = 6.8 and 7.7 K. for Co-*N*-Sali-COO and Co-*N*-Sali-SO_3 respectively.

Despite the absence of *in-situ cis-trans* photoisomerization of *N*-Sali-R, this study allows to better understand and uncover the difficulties in actuating such photoisomerization inside LSHs. Notably, it shows that the ESIPT mechanism is efficient in Zn hybrid LSHs providing new luminescent hybrid materials with high thermal stability. Moreover, it paves the way for the design of new multifunctional materials, combining interesting magnetic and optical properties. One strategy we are currently following is to optimize the controlled co-insertion of *N*-Sali-R anions along with long alkyl chain anions; in order to break the intermolecular interactions between the *N*-Sali-R molecules that might allow a larger open space for the *cis-trans* pedal movement to take place.

AUTHOR INFORMATION

Corresponding Authors

Institut de Physique et Chimie de Strasbourg, CNRS – Université de Strasbourg, UMR7504, 23 rue du Loess, 67034 Strasbourg cedex 2, France

varun.kumar@ipcms.unistra.fr

rogez@unistra.fr

Present Addresses

† Advance Research Center for NanoLithography, Science Park 106, 1098XG Amsterdam, The Netherlands.

Author Contributions

The manuscript was written through contributions of all authors. All authors have given approval to the final version of the manuscript.

ACKNOWLEDGMENT

The authors thank the CNRS, the Université de Strasbourg and the the Agence Nationale de la Recherche (Contract No. ANR-14-CE07-0004-01 (HYMN)). The Wallonie – Bruxelles International is gratefully acknowledged for a WBI-World grant to VK. The MEB-Cro and XRD facility platforms are acknowledged for access to the SEM and X-Ray diffractometer. The authors thank D. Burger, C. Kiefer, M.-N. Lalloz, L. Mager and D. Cianfarani for technical assistance.

REFERENCES

(1) Osada, M.; Sasaki, T. Nanoarchitectonics in Dielectric/Ferroelectric Layered Perovskites: From Bulk 3D Systems to 2D Nanosheets. *Dalton Trans.* **2018**, *47* (9), 2841–2851. https://doi.org/10.1039/C7DT03719H.

(2) Jin, X.; Gu, T.-H.; Kwon, N. H.; Hwang, S.-J. Synergetic Advantages of Atomically Coupled 2D Inorganic and Graphene Nanosheets as Versatile Building Blocks for Diverse Functional Nanohybrids. *Adv. Mater.* **2021**, *33* (47), 2005922. https://doi.org/10.1002/adma.202005922.

(3) *Functional Hybrid Materials*; Gómez-Romero, P., Sanchez, C., Eds.; Wiley-VCH: Weinheim, 2004.

(4) Li, M.; Mann, S. Emergent Hybrid Nanostructures Based on Non-Equilibrium Block Copolymer Self-Assembly. *Angew. Chem. Int. Ed.* **2008**, *47* (49), 9476–9479.

(5) Sanchez, C.; Belleville, P.; Popall, M.; Nicole, L. Applications of Advanced Hybrid Organic–Inorganic Nanomaterials: From Laboratory to Market. *Chem. Soc. Rev.* **2011**, *40* (2), 696–753. https://doi.org/10.1039/C0CS00136H.

(6) Faustini, M.; Nicole, L.; Ruiz-Hitzky, E.; Sanchez, C. History of Organic–Inorganic Hybrid Materials: Prehistory, Art, Science, and Advanced Applications. *Adv. Funct. Mater.* **2018**, *28* (27), 1704158. https://doi.org/10.1002/adfm.201704158.

(7) Rogez, G.; Massobrio, C.; Rabu, P.; Drillon, M. Layered Hydroxide Hybrid Nanostructures: A Route to Multifunctionality. *Chem. Soc. Rev.* **2011**, *40* (2), 1031–1058. https://doi.org/10.1039/C0CS00159G.

(8) Fernandes, F. M.; Baradari, H.; Sanchez, C. Integrative Strategies to Hybrid Lamellar Compounds: An Integration Challenge. *Appl. Clay Sci.* **2014**, *100*, 2–21. https://doi.org/10.1016/j.clay.2014.05.013.
(9) Abellán, G.; Martí-Gastaldo, C.; Ribera, A.; Coronado, E. Hybrid Materials Based on Magnetic Layered Double Hydroxides: A Molecular Perspective. *Acc. Chem. Res.* **2015**, *48* (6), 1601–1611. https://doi.org/10.1021/acs.accounts.5b00033.
(10) Uppuluri, R.; Gupta, A. S.; Rosas, A. S.; Mallouk, T. E. Soft Chemistry of Ion-Exchangeable Layered Metal Oxides. *Chem. Soc. Rev.* **2018**, *47* (7), 2401–2430. https://doi.org/10.1039/C7CS00290D.
(11) Shi, H.; He, J. Orientated Intercalation of Tartrate as Chiral Ligand to Impact Asymmetric Catalysis. *J. Catal.* **2011**, *279* (1), 155–162. https://doi.org/10.1016/j.jcat.2011.01.012.
(12) Gastaldi, C.; Taviot-Guého, C.; Guérard-Hélaine, C.; Forano, C. NHC-Heterocycle Carbene Gold Catalyst Intercalated in Layered Double Hydroxides as Reusable Hybrid Catalyst in Acidic Medium. *Appl. Clay Sci.* **2023**, *238*, 106931. https://doi.org/10.1016/j.clay.2023.106931.
(13) Huang, H.; Song, S.; Shuai, C.-X.; Xu, Q.-C.; Jiang, Y. Layered Double Hydroxide-Polyaniline Nanofibers in Lightweight Aerogels for Bioinspired Flame-Retardant Wood. *ACS Appl. Nano Mater.* **2023**, *6* (6), 4105–4111. https://doi.org/10.1021/acsanm.3c00195.
(14) Conterosito, E.; Benesperi, I.; Toson, V.; Saccone, D.; Barbero, N.; Palin, L.; Barolo, C.; Gianotti, V.; Milanesio, M. High-Throughput Preparation of New Photoactive Nanocomposites. *ChemSusChem* **2016**, *9* (11), 1279–1289. https://doi.org/10.1002/cssc.201600325.
(15) Lee, J. H.; Chang, J.; Cha, J.-H.; Jung, D.-Y.; Kim, S. S.; Kim, J. M. Anthraquinone Sulfonate Modified, Layered Double Hydroxide Nanosheets for Dye-Sensitized Solar Cells. *Chem. Eur. J.* **2010**, *16* (28), 8296–8299. https://doi.org/10.1002/chem.201000703.
(16) Wang, Q.; Tay, H. H.; Guo, Z.; Chen, L.; Liu, Y.; Chang, J.; Zhong, Z.; Luo, J.; Borgna, A. Morphology and Composition Controllable Synthesis of Mg–Al–CO3 Hydrotalcites by Tuning the Synthesis pH and the CO_2 Capture Capacity. *Appl. Clay Sci.* **2012**, *55*, 18–26. https://doi.org/10.1016/j.clay.2011.07.024.
(17) Yu, S.; Choi, G.; Choy, J.-H. Multifunctional Layered Double Hydroxides for Drug Delivery and Imaging. *Nanomaterials* **2023**, *13* (6), 1102. https://doi.org/10.3390/nano13061102.
(18) Silva, E. H. C.; Cutrim, E. S. M.; Iemma, M. R. C.; Barud, H. S.; Rojas, A.; Gómez-Hortigüela, L.; Menezes, A. S. de; Rodríguez-Castellón, E.; Tanaka, A. A.; Alcântara, A. C. S. New Insights about the Intercalation of 5-Fluorouracil into 2D Mg–Al Layered Double Hydroxide Nanosheets: A Theoretical and Experimental Investigation. *J. Drug Deliv. Sci. Technol.* **2023**, *81*, 104294. https://doi.org/10.1016/j.jddst.2023.104294.
(19) Hou, Z.; Yu, J.; Zhou, X.; Chen, Z.; Xu, J.; Zhao, B.; Gen, W.; Zhang, H. Enhanced Performance of Hybrid Supercapacitors by the Synergistic Effect of $Co(OH)_2$ Nanosheets and NiMn Layered Hydroxides. *J. Colloid Interf. Sci.* **2023**, *646*, 753–762. https://doi.org/10.1016/j.jcis.2023.05.128.
(20) Ali, S.; Marwat, M. A.; Khan, M. F.; Adam, K. M.; Din, Z. U.; Karim, M. R. A.; Khan, S. Ti_3SiC_2-Coupled NiCoMn LDH Nanocomposites as Positive Electrode for High Performance Supercapacitors. *J. Alloy. Compd.* **2023**, *956*, 170229. https://doi.org/10.1016/j.jallcom.2023.170229.
(21) Abellán, G.; Coronado, E.; Martí-Gastaldo, C.; Ribera, A.; Jordá, J. L.; García, H. Photo-Switching in a Hybrid Material Made of Magnetic Layered Double Hydroxides Intercalated with Azobenzene Molecules. *Adv. Mater.* **2014**, *26* (24), 4156–4162. https://doi.org/10.1002/adma.201400713.
(22) Taviot-Guého, C.; Prévot, V.; Forano, C.; Renaudin, G.; Mousty, C.; Leroux, F. Tailoring Hybrid Layered Double Hydroxides for the Development of Innovative Applications. *Adv. Funct. Mater.* **2018**, *28* (27), 1703868. https://doi.org/10.1002/adfm.201703868.
(23) Train, C.; Gheorghe, R.; Krstic, V.; Chamoreau, L.-M.; Ovanesyan, N. S.; Rikken, G. L. J. A.; Gruselle, M.; Verdaguer, M. Strong Magneto-Chiral Dichroism in Enantiopure Chiral Ferromagnets. *Nat. Mater.* **2008**, *7* (9), 729–734. https://doi.org/10.1038/nmat2256.

(24) Pardo, E.; Train, C.; Liu, H.; Chamoreau, L.-M.; Dkhil, B.; Boubekeur, K.; Lloret, F.; Nakatani, K.; Tokoro, H.; Ohkoshi, S.; Verdaguer, M. Multiferroics by Rational Design: Implementing Ferroelectricity in Molecule-Based Magnets. *Angew. Chem. Int. Ed.* **2012**, *51* (33), 8356–8360. https://doi.org/10.1002/anie.201202848.

(25) Coronado, E.; Galán-Mascarós, J. R.; Gómez-García, C. J.; Laukhin, V. Coexistence of Ferromagnetism and Metallic Conductivity in a Molecule-Based Layered Compound. *Nature* **2000**, *408* (6811), 447–449. https://doi.org/10.1038/35044035.

(26) Lacroix, P. G.; Clément, R.; Nakatani, K.; Zyss, J.; Ledoux, I. Stilbazolium-MPS_3 Nanocomposites with Large Second-Order Optical Nonlinearity and Permanent Magnetization. *Science* **1994**, *263* (5147), 658–660. https://doi.org/10.1126/science.263.5147.658.

(27) Lacroix, P. G.; Malfant, I.; Bénard, S.; Yu, P.; Rivière, E.; Nakatani, K. Hybrid Molecular-Based Magnets Containing Organic NLO Chromophores: A Search toward an Interplay between Magnetic and NLO Behavior. *Chem. Mater.* **2001**, *13* (2), 441–449. https://doi.org/10.1021/cm001177v.

(28) Catti, M.; Ferraris, G.; Hull, S.; Pavese, A. Static Compression and H Disorder in Brucite, $Mg(OH)_2$, to 11 GPa: A Powder Neutron Diffraction Study. *Phys. Chem. Minerals* **1995**, *22* (3), 200–206. https://doi.org/10.1007/BF00202300.

(29) Louër, M.; Louër, D.; Grandjean, D. Etude Structurale Des Hydroxynitrates de Nickel et de Zinc. I. Classification Structurale. *Acta Cryst. Sect. B* **1973**, *29*, 1696–1703.

(30) Švarcová, S.; Klementová, M.; Bezdička, P.; Łasocha, W.; Dušek, M.; Hradil, D. Synthesis and Characterization of Single Crystals of the Layered Copper Hydroxide Acetate $Cu_2(OH)_3(CH_3COO)\cdot H_2O$. *Cryst. Res. Technol.* **2011**, *46* (10), 1051–1057. https://doi.org/10.1002/crat.201100262.

(31) Evrard, Q.; Leuvrey, C.; Farger, P.; Delahaye, E.; Rabu, P.; Taupier, G.; Dorkenoo, K. D.; Rueff, J.-M.; Barrier, N.; Pérez, O.; Rogez, G. Noncentrosymmetric Cu(II) Layered Hydroxide: Synthesis, Crystal Structure, Nonlinear Optical, and Magnetic Properties of $Cu_2(OH)_3(C_{12}H_{25}SO_4)$. *Cryst. Growth Des.* **2018**, *18* (3), 1809–1817. https://doi.org/10.1021/acs.cgd.7b01692.

(32) Neilson, J. R.; Kurzman, J. A.; Seshadri, R.; Morse, D. E. Cobalt Coordination and Clustering in α-$Co(OH)_2$ Revealed by Synchrotron X-Ray Total Scattering. *Chem. Eur. J.* **2010**, *16* (33), 9998–10006. https://doi.org/10.1002/chem.201000661.

(33) Neilson, J. R.; Schwenzer, B.; Seshadri, R.; Morse, D. E. Kinetic Control of Intralayer Cobalt Coordination in Layered Hydroxides: Co1−0.5xoctCoxtet(OH)2(Cl)x(H2O)n. *Inorg. Chem.* **2009**, *48* (23), 11017–11023. https://doi.org/10.1021/ic901167u.

(34) Neilson, J. R.; Morse, D. E.; Melot, B. C.; Shoemaker, D. P.; Kurzman, J. A.; Seshadri, R. Understanding Complex Magnetic Order in Disordered Cobalt Hydroxides through Analysis of the Local Structure. *Phys. Rev. B* **2011**, *83* (9), 094418. https://doi.org/10.1103/PhysRevB.83.094418.

(35) Ma, R.; Liu, Z.; Takada, K.; Fukuda, K.; Ebina, Y.; Bando, Y.; Sasaki, T. Tetrahedral Co(II) Coordination in α-Type Cobalt Hydroxide: Rietveld Refinement and X-Ray Absorption Spectroscopy. *Inorg. Chem.* **2006**, *45* (10), 3964–3969. https://doi.org/10.1021/ic052108r.

(36) Stählin, W.; Oswald, H. R. The Crystal Structure of Zinc Hydroxide Nitrate, $Zn_5(OH)_8(NO_3)_2.2H_2O$. *Acta Cryst. Sect. B* **1970**, *26*, 860–863.

(37) Laget, V.; Hornick, C.; Rabu, P.; Drillon, M.; Ziessel, R. Molecular Magnets: Hybrid Organic–Inorganic Layered Compounds with Very Long-Range Ferromagnetism. *Coord. Chem. Rev.* **1998**, *178–180*, 1533–1553. https://doi.org/10.1016/S0010-8545(98)00166-0.

(38) Hornick, C.; Rabu, P.; Drillon, M. Hybrid Organic–Inorganic Multilayer Materials: Influence of π Electrons as Magnetic Media in a Series of Bridged-Layer Compounds $M_2(OH)_{4-x}A_{x/2}$ (M=Cu(II) or Co(II), A=dicarboxylate Anion). *Polyhedron* **2000**, *19* (3), 259–266. https://doi.org/10.1016/S0277-5387(99)00355-1.

(39) Rabu, P.; Rouba, S.; Laget, V.; Hornick, C.; Drillon, M. Ferro/Antiferromagnetism Mediated by Interlayer Organic Spacers in Layered Copper(II) Compounds. *Chem. Commun.* **1996**, *0* (10), 1107–1108. https://doi.org/10.1039/CC9960001107.
(40) Oestreicher, V.; Hunt, D.; Dolle, C.; Borovik, P.; Jobbágy, M.; Abellán, G.; Coronado, E. The Missing Link in the Magnetism of Hybrid Cobalt Layered Hydroxides: The Odd–Even Effect of the Organic Spacer. *Chem. Eur. J.* **2021**, *27* (3), 921–927. https://doi.org/10.1002/chem.202003593.
(41) Oestreicher, V.; Dolle, C.; Hunt, D.; Fickert, M.; Abellán, G. Room Temperature Synthesis of Two-Dimensional Multilayer Magnets Based on α-CoII Layered Hydroxides. *Nano Mater. Sci.* **2022**, *4* (1), 36–43. https://doi.org/10.1016/j.nanoms.2020.12.004.
(42) Park, S.-H.; Lee, C. E. Layered Copper Hydroxide N-Alkylsulfonate Salts: Synthesis, Characterization, and Magnetic Behaviors in Relation to the Basal Spacing. *J. Phys. Chem. B* **2005**, *109* (3), 1118–1124. https://doi.org/10.1021/jp046902u.
(43) Delahaye, É.; Eyele-Mezui, S.; Bardeau, J.-F.; Leuvrey, C.; Mager, L.; Rabu, P.; Rogez, G. New Layered Organic-Inorganic Magnets Incorporating Azo Dyes. *J. Mater. Chem.* **2009**, *19* (34), 6106–6115. https://doi.org/10.1039/B905557F.
(44) Demessence, A.; Yassar, A.; Rogez, G.; Miozzo, L.; De Brion, S.; Rabu, P. Synthesis, Optical and Magnetic Properties of Hybrid α, α'-Oligothiophenecarboxylates/Transition Metal Hydroxide Multilayered Compounds. *J. Mater. Chem.* **2010**, *20* (42), 9401–9414. https://doi.org/10.1039/B927117A.
(45) Demessence, A.; Rogez, G.; Rabu, P. Grafting of Thiophenecarboxylates into Magnetic Transition Metal Hydroxide Layers. *Chem. Mater.* **2006**, *18* (13), 3005–3015. https://doi.org/10.1021/cm060366w.
(46) Rueff, J.-M.; Nierengarten, J.-F.; Gilliot, P.; Demessence, A.; Cregut, O.; Drillon, M.; Rabu, P. Influence of Magnetic Ordering on the Luminescence in a Layered Organic−Inorganic OPV−Ni(II) Compound. *Chem. Mater.* **2004**, *16* (15), 2933–2937. https://doi.org/10.1021/cm049792c.
(47) Evrard, Q.; Chaker, Z.; Roger, M.; Sevrain, C. M.; Delahaye, E.; Gallart, M.; Gilliot, P.; Leuvrey, C.; Rueff, J.-M.; Rabu, P.; Massobrio, C.; Boero, M.; Pautrat, A.; Jaffrès, P.-A.; Ori, G.; Rogez, G. Layered Simple Hydroxides Functionalized by Fluorene-Phosphonic Acids: Synthesis, Interface Theoretical Insights, and Magnetoelectric Effect. *Adv. Funct. Mater.* **2017**, 1703576. https://doi.org/10.1002/adfm.201703576.
(48) Bourzami, R.; Eyele-Mezui, S.; Delahaye, E.; Drillon, M.; Rabu, P.; Parizel, N.; Choua, S.; Turek, P.; Rogez, G. New Metal Phthalocyanines/Metal Simple Hydroxide Multilayers: Experimental Evidence of Dipolar Field-Driven Magnetic Behavior. *Inorg. Chem.* **2014**, *53* (2), 1184–1194. https://doi.org/10.1021/ic4027688.
(49) Delahaye, É.; Eyele-Mezui, S.; Diop, M.; Leuvrey, C.; Rabu, P.; Rogez, G. Rational Synthesis of Chiral Layered Magnets by Functionalization of Metal Simple Hydroxides with Chiral and Non-Chiral Ni(II) Schiff Base Complexes. *Dalton Trans.* **2010**, *39* (44), 10577–10580. https://doi.org/10.1039/C0DT00834F.
(50) Eyele-Mezui, S.; Delahaye, E.; Rogez, G.; Rabu, P. Functional Hybrid Materials Based on Layered Simple Hydroxide Hosts and Dicarboxylate Schiff Base Metal Complex Guests. *Eur. J. Inorg. Chem.* **2012**, No. 32, 5225–5238. https://doi.org/10.1002/ejic.201200695.
(51) Delahaye, E.; Eyele-Mezui, S.; Diop, M.; Leuvrey, C.; Foix, D.; Gonbeau, D.; Rabu, P.; Rogez, G. Functional Heterometallic Layered Hybrid Magnets by Double Ion-Exchange. *Eur. J. Inorg. Chem.* **2012**, No. 16, 2731–2740.
(52) Abellán, G.; Jordá, J. L.; Atienzar, P.; Varela, M.; Jaafar, M.; Gómez-Herrero, J.; Zamora, F.; Ribera, A.; García, H.; Coronado, E. Stimuli-Responsive Hybrid Materials: Breathing in Magnetic Layered Double Hydroxides Induced by a Thermoresponsive Molecule. *Chem. Sci.* **2015**, *6* (3), 1949–1958. https://doi.org/10.1039/C4SC03460K.

(53) Hadjoudis, E.; Mavridis, I. M. Photochromism and Thermochromism of Schiff Bases in the Solid State: Structural Aspects. *Chem. Soc. Rev.* **2004**, *33* (9), 579–588. https://doi.org/10.1039/B303644H.
(54) Jacquemin, P.-L.; Robeyns, K.; Devillers, M.; Garcia, Y. Reversible Photochromism of an N-Salicylidene Aniline Anion. *Chem. Commun.* **2014**, *50* (6), 649–651. https://doi.org/10.1039/C3CC45080E.
(55) Plaquet, A.; Guillaume, M.; Champagne, B.; Rougier, L.; Mançois, F.; Rodriguez, V.; Pozzo, J.-L.; Ducasse, L.; Castet, F. Investigation on the Second-Order Nonlinear Optical Responses in the Keto−Enol Equilibrium of Anil Derivatives. *J. Phys. Chem. C* **2008**, *112* (14), 5638–5645. https://doi.org/10.1021/jp711511t.
(56) Baleizão, C.; Garcia, H. Chiral Salen Complexes: An Overview to Recoverable and Reusable Homogeneous and Heterogeneous Catalysts. *Chem. Rev.* **2006**, *106* (9), 3987–4043.
(57) Sunil, K.; Kumara, T. P. P.; Kumar, B. A.; Patel, S. B. Synthesis, Characterization and Antiioxidant Activity of Schiff Base Compounds Obtained Using Green Chemistry Techniques. *Pharm. Chem. J.* **2021**, *55* (1), 46–53. https://doi.org/10.1007/s11094-021-02370-8.
(58) Cimerman, Z.; Galic, N.; Bosner, B. The Schiff Bases of Salicylaldehyde and Aminopyridines as Highly Sensitive Analytical Reagents. *Anal. Chim. Acta* **1997**, *343* (1), 145–153. https://doi.org/10.1016/S0003-2670(96)00587-9.
(59) Jochum, F. D.; Theato, P. Temperature- and Light-Responsive Polyacrylamides Prepared by a Double Polymer Analogous Reaction of Activated Ester Polymers. *Macromolecules* **2009**, *42* (16), 5941–5945. https://doi.org/10.1021/ma900945s.
(60) Kawata, S.; Kawata, Y. Three-Dimensional Optical Data Storage Using Photochromic Materials. *Chem. Rev.* **2000**, *100* (5), 1777–1788. https://doi.org/10.1021/cr980073p.
(61) Sugiyama, H.; Johmoto, K.; Sekine, A.; Uekusa, H. In-Situ Photochromism Switching with Crystal Jumping through the Deammoniation of N-Salicylideneaniline Ammonium Salt. *Cryst. Growth Des.* **2019**, *19* (8), 4324–4331. https://doi.org/10.1021/acs.cgd.9b00039.
(62) Laget, V.; Hornick, C.; Rabu, P.; Drillon, M. Hybrid Organic-Inorganic Layered Compounds Prepared by Anion Exchange Reaction: Correlation between Structure and Magnetic Properties. *J. Mater. Chem.* **1999**, *9* (1), 169–174. https://doi.org/10.1039/A805870I.
(63) Demel, J.; Pleštil, J.; Bezdička, P.; Janda, P.; Klementová, M.; Lang, K. Few-Layer ZnO Nanosheets: Preparation, Properties, and Films with Exposed {001} Facets. *J. Phys. Chem. C* **2011**, *115*, 24702–24706.
(64) Park, S.-H.; Jung, M.-H.; Lee, Y.-J.; Huh, Y.-D. Confined Condensation Synthesis and Magnetic Properties of Layered Copper Hydroxide Frameworks. *Dalton Trans.* **2017**, *46* (10), 3363–3368. https://doi.org/10.1039/C7DT00071E.
(65) Palamarciuc, O.; Delahaye, E.; Rabu, P.; Rogez, G. Microwave-Assisted Post-Synthesis Modification of Layered Simple Hydroxides. *New J. Chem.* **2014**, *38* (5), 2016–2023. https://doi.org/10.1039/C3NJ01231J.
(66) Bellobono, I. R.; Favini, G. Rate of Hydrolysis of N-Salicylideneaniline in Water–Methanol Solutions. *J. Chem. Phys.* **2003**, *48* (12), 5738–5740. https://doi.org/10.1063/1.1668673.
(67) Dash, A. C.; Nanda, R. K. Reactions of Coordinated Ligands. I. Kinetics and Mechanism of Hydrolysis of N-Salicylideneaniline in the Presence of Metal Ions. *J. Am. Chem. Soc.* **1969**, *91* (25), 6944–6947. https://doi.org/10.1021/ja01053a010.
(68) Demel, J.; Kubát, P.; Jirka, I.; Kovář, P.; Pospíšil, M.; Lang, K. Inorganic−Organic Hybrid Materials: Layered Zinc Hydroxide Salts with Intercalated Porphyrin Sensitizers. *J. Phys. Chem. C* **2010**, *114* (39), 16321–16328. https://doi.org/10.1021/jp106116n.
(69) Eyele-Mezui, S.; Vialat, P.; Higy, C.; Bourzami, R.; Leuvrey, C.; Parizel, N.; Turek, P.; Rabu, P.; Rogez, G.; Mousty, C. Electrocatalytic Properties of Metal Phthalocyanine Tetrasulfonate Intercalated in

Metal Layered Simple Hydroxides (Metal: Co, Cu, and Zn). *J. Phys. Chem. C* **2015**, *119* (23), 13335–13342. https://doi.org/10.1021/acs.jpcc.5b02985.

(70) Deacon, G. B.; Phillips, R. J. Relationships between the Carbon-Oxygen Stretching Frequencies of Carboxylato Complexes and the Type of Carboxylate Coordination. *Coord. Chem. Rev.* **1980**, *33* (3), 227–250.

(71) Dendrinou-Samara, C.; Tsotsou, G.; Ekateriniadou, L. V.; H. Kortsaris, A.; Raptopoulou, C. P.; Terzis, A.; Kyriakidis, D. A.; Kessissoglou, D. P. Anti-Inflammatory Drugs Interacting with Zn(II), Cd(II) and Pt(II) Metal Ions. *J. Inorg. Biochem.* **1998**, *71* (3), 171–179. https://doi.org/10.1016/S0162-0134(98)10051-X.

(72) Drożdżewski, P.; Brożyna, A.; Kubiak, M. New Binuclear Copper(II) Complex with 2-Thiopheneacetic Acid. Synthesis, X-Ray Diffraction and Vibrational Studies of Bis(N,N-Dimethylformamide)Tetra(2-Thiopheneacetato)Dicopper(II). *J. Mol. Struct.* **2004**, *707* (1–3), 131.

(73) Nara, M.; Torii, H.; Tasumi, M. Correlation between the Vibrational Frequencies of the Carboxylate Group and the Types of Its Coordination to a Metal Ion: An Ab Initio Molecular Orbital Study. *J. Phys. Chem.* **1996**, *100* (51), 19812–19817. https://doi.org/10.1021/jp9615924.

(74) Robert, V.; Lemercier, G. A Combined Experimental and Theoretical Study of Carboxylate Coordination Modes: A Structural Probe. *J. Am. Chem. Soc.* **2006**, *128* (4), 1183–1187. https://doi.org/10.1021/ja055121j.

(75) Rodriguez-Carvajal, J. Recent Advances in Magnetic Structure Determination by Neutron Powder Diffraction. *Physica B: Condensed Matter* **1993**, *192* (1–2), 55–69. https://doi.org/doi:10.1016/0921-4526(93)90108-I.

(76) Sun, Z.; Jin, L.; Shi, W.; Wei, M.; Evans, D. G.; Duan, X. Controllable Photoluminescence Properties of an Anion-Dye-Intercalated Layered Double Hydroxide by Adjusting the Confined Environment. *Langmuir* **2011**, *27* (11), 7113–7120. https://doi.org/10.1021/la200846j.

(77) Yang, J.-H.; Han, Y.-S.; Park, M.; Park, T.; Hwang, S.-J.; Choy, J.-H. New Inorganic-Based Drug Delivery System of Indole-3-Acetic Acid-Layered Metal Hydroxide Nanohybrids with Controlled Release Rate. *Chem. Mater.* **2007**, *19* (10), 2679–2685. https://doi.org/10.1021/cm070259h.

(78) Demel, J.; Hynek, J.; Kovář, P.; Dai, Y.; Taviot-Guého, C.; Demel, O.; Pospíšil, M.; Lang, K. Insight into the Structure of Layered Zinc Hydroxide Salts Intercalated with Dodecyl Sulfate Anions. *J. Phys. Chem. C* **2014**, *118* (46), 27131–27141. https://doi.org/10.1021/jp508499g.

(79) Johmoto, K.; Sekine, A.; Uekusa, H. Photochromism Control of Salicylideneaniline Derivatives by Acid–Base Co-Crystallization. *Cryst. Growth Des.* **2012**, *12* (10), 4779–4786. https://doi.org/10.1021/cg300454q.

(80) Masciocchi, N.; Corradi, E.; Sironi, A.; Moretti, G.; Minelli, G.; Porta, P. Preparation, Characterization, and Ab initioX-Ray Powder Diffraction Study of $Cu_2(OH)_3(CH3COO)\cdot H_2O$. *J. Solid State Chem.* **1997**, *131* (2), 252–262. https://doi.org/10.1006/jssc.1997.7372.

(81) Poul, L.; Jouini, N.; Fiévet, F. Layered Hydroxide Metal Acetates (Metal = Zinc, Cobalt, and Nickel): Elaboration via Hydrolysis in Polyol Medium and Comparative Study. *Chem. Mater.* **2000**, *12* (10), 3123–3132. https://doi.org/10.1021/cm991179j.

(82) Taibi, M.; Ammar, S.; Jouini, N.; Fiévet, F.; Molinié, P.; Drillon, M. Layered Nickel Hydroxide Salts: Synthesis, Characterization and Magnetic Behaviour in Relation to the Basal Spacing. *J. Mater. Chem.* **2002**, *12*, 3238–3244.

(83) Oriakhi, C. O.; Farr, I. V.; Lerner, M. M. Incorporation of Poly(Acrylic Acid), Poly(Vinylsulfonate) and Poly(Styrenesulfonate) within Layered Double Hydroxides. *J. Mater. Chem.* **1996**, *6* (1), 103–107. https://doi.org/10.1039/JM9960600103.

(84) Hadjoudis, E.; Verganelakis, V.; Trapalis, C.; Kordas, G. Environmental Effect of Sol-Gel Encapsulation on Photochromic and Thermochromic Anils. *Molecular Engineering* **1999**, *8* (4), 459–469. https://doi.org/10.1023/A:1008310718276.

(85) Amimoto, K.; Kawato, T. Photochromism of Organic Compounds in the Crystal State. *J. Photochem. Photobiol. C: Photochem. Rev.* **2005**, *6* (4), 207–226. https://doi.org/10.1016/j.jphotochemrev.2005.12.002.
(86) Ziółek, M.; Sobczak, I. Photochromism and Hydrolysis of Aromatic Schiff Base N,N'-Bis(Salicylidene)-p-Phenylenediamine (BSP) Studied in Heterogeneous Environments. *J Incl. Phenom. Macrocycl. Chem.* **2009**, *63* (3), 211–218. https://doi.org/10.1007/s10847-008-9509-2.
(87) Fujiwara, T.; Harada, J.; Ogawa, K. Solid-State Thermochromism Studied by Variable-Temperature Diffuse Reflectance Spectroscopy. A New Perspective on the Chromism of Salicylideneanilines. *J. Phys. Chem. B* **2004**, *108* (13), 4035–4038. https://doi.org/10.1021/jp037438g.
(88) Robert, F.; Naik, A. D.; Tinant, B.; Garcia, Y. N-Salicylidene Anil Anions as Thermo-Sensitive Components of Organic–Inorganic Hybrid Materials. *Inorg. Chim. Acta* **2012**, *380*, 104–113. https://doi.org/10.1016/j.ica.2011.08.040.
(89) Lever, A. B. P. *Inorganic Electronic Spectroscopy, 2nd Edition*; Elsevier: Amsterdam, 1984.
(90) Lever, A. B. P. Electronic Spectra of Some Transition Metal Complexes: Derivation of Dq and B. *J. Chem. Educ.* **1968**, *45* (11), 711. https://doi.org/10.1021/ed045p711.
(91) Dou, Y. Equations for Calculating Dq and B. *J. Chem. Educ.* **1990**, *67* (2), 134. https://doi.org/10.1021/ed067p134.
(92) Avadanei, M.; Cozan, V.; Shova, S.; Paixão, J. A. Solid State Photochromism and Thermochromism of Two Related N-Salicylidene Anilines. *Chem. Phys.* **2014**, *444*, 43–51. https://doi.org/10.1016/j.chemphys.2014.10.007.
(93) Sliwa, M.; Mouton, N.; Ruckebusch, C.; Aloïse, S.; Poizat, O.; Buntinx, G.; Métivier, R.; Nakatani, K.; Masuhara, H.; Asahi, T. Comparative Investigation of Ultrafast Photoinduced Processes in Salicylidene-Aminopyridine in Solution and Solid State. *J. Phys. Chem. C* **2009**, *113* (27), 11959–11968. https://doi.org/10.1021/jp901849a.
(94) Sugiyama, H. Crystal Structures and Thermochromic and Fluorescence Properties of N-Salicylideneaniline Derivatives Having a Naphthyl-Isoquinoline Group. *J. Mol. Struct.* **2021**, *1229*, 129603. https://doi.org/10.1016/j.molstruc.2020.129603.
(95) Casades, I.; Álvaro, M.; García, H.; Pillai, M. N. Photochemistry of Anils in NaY Zeolite. *European Journal of Organic Chemistry* **2002**, *2002* (13), 2074–2079. https://doi.org/10.1002/1099-0690(200207)2002:13<2074::AID-EJOC2074>3.0.CO;2-I.
(96) Juribašić, M.; Bregović, N.; Stilinović, V.; Tomišić, V.; Cindrić, M.; Šket, P.; Plavec, J.; Rubčić, M.; Užarević, K. Supramolecular Stabilization of Metastable Tautomers in Solution and the Solid State. *Chem. Eur. J.* **2014**, *20* (52), 17333–17345. https://doi.org/10.1002/chem.201403543.
(97) Hureau, M.; Moissette, A.; Smirnov, K. S. A Spectroscopic Study of Tautomeric Equilibrium of Salicylideneaniline in ZSM-5 Zeolites. *Molecules* **2019**, *24* (4), 795. https://doi.org/10.3390/molecules24040795.
(98) Ogawa, K.; Kasahara, Y.; Ohtani, Y.; Harada, J. Crystal Structure Change for the Thermochromy of N-Salicylideneanilines. The First Observation by X-Ray Diffraction. *J. Am. Chem. Soc.* **1998**, *120* (28), 7107–7108. https://doi.org/10.1021/ja980972v.
(99) Hulushe, S. T.; Malan, F. P.; Hosten, E. C.; Lobb, K. A.; Khanye, S. D.; Watkins, G. M. Photo-and Thermoresponsive N-Salicylideneaniline Derivatives: Solid-State Studies and Structural Aspects. *New J. Chem.* **2022**, *46* (43), 20940–20950. https://doi.org/10.1039/D1NJ03056F.
(100) Robert, F.; Jacquemin, P.-L.; Tinant, B.; Garcia, Y. Trans-Keto* Form Detection in Non Photochromic N-Salicylidene Aminomethylpyridines. *CrystEngComm* **2012**, *14* (13), 4396–4406. https://doi.org/10.1039/C2CE00006G.
(101) Mittapalli, S.; Sravanakumar Perumalla, D.; Nangia, A. Mechanochemical Synthesis of N-Salicylidene-aniline: Thermosalient Effect of Polymorphic Crystals. *IUCrJ* **2017**, *4* (3), 243–250. https://doi.org/10.1107/S2052252517004043.

(102) Carlin, R. L. *Magnetochemistry*; Springer-Verlag: Berlin, 1986.
(103) Drillon, M.; Panissod, P. Long-Range Ferromagnetism in Hybrid Compounds: The Role of Dipolar Interactions. *J. Magn. Magn. Mater.* **1998**, *188* (1–2), 93–99. https://doi.org/10.1016/S0304-8853(98)00180-2.